Available online at www.sciencedirect.com
ScienceDirect
Journal of Computational Physics 221 (2007) 395–421
JOURNAL OF COMPUTATIONAL PHYSICS
www.elsevier.com/locate/jcp

An extended level set method for shape and topology optimization

S.Y. Wang [a,*], K.M. Lim [a,b], B.C. Khoo [a,b], M.Y. Wang [c]

[a] Centre for Singapore-MIT Alliance, National University of Singapore, E4-04-10, 4 Engineering Drive 3, Singapore 117576, Singapore
[b] Department of Mechanical Engineering, National University of Singapore, Singapore 119260, Singapore
[c] Department of Automation and Computer-Aided Engineering, The Chinese University of Hong Kong, Shatin, NT, Hong Kong

Received 30 November 2005; received in revised form 3 May 2006; accepted 15 June 2006
Available online 4 August 2006

Abstract

In this paper, the conventional level set methods are extended as an effective approach for shape and topology optimization by the introduction of the radial basis functions (RBFs). The RBF multiquadric splines are used to construct the implicit level set function with a high level of accuracy and smoothness and to discretize the original initial value problem into an interpolation problem. The motion of the dynamic interfaces is thus governed by a system of coupled ordinary differential equations (ODEs) and a relatively smooth evolution can be maintained without reinitialization. A practical implementation of this method is further developed for solving a class of energy-based optimization problems, in which approximate solution to the original Hamilton–Jacobi equation may be justified and nucleation of new holes inside the material domain is allowed for. Furthermore, the severe constraints on the temporal and spatial discretizations can be relaxed, leading to a rapid convergence to the final design insensitive to initial guesses. The normal velocities are chosen to perform steepest gradient-based optimization by using shape sensitivity analysis and a bi-sectioning algorithm. A physically meaningful and efficient extension velocity method is also presented. The proposed method is implemented in the framework of minimum compliance design and its efficiency over the existing methods is highlighted. Numerical examples show its accuracy, convergence speed and insensitivity to initial designs in shape and topology optimization of two-dimensional (2D) problems that have been extensively investigated in the literature.

Keywords: Topology optimization; Shape optimization; Level set method; Radial basis functions; Extension velocity; Gradient-based optimization

1. Introduction

The level set method first introduced and devised by Osher and Sethian [1] in 1988 is a simple and versatile method for computing and analyzing the motion of an interface in two or three dimensions and following the evolution of interfaces. Since these interfaces may easily develop sharp corners, break apart, and merge

* Corresponding author. Tel.: +65 6874 8934; fax: +65 6775 2920.
E-mail addresses: smaws@nus.edu.sg, dr.sywang@gmail.com (S.Y. Wang).

0021-9991/$ - see front matter © 2006 Elsevier Inc. All rights reserved.
doi:10.1016/j.jcp.2006.06.029

together in a robust and stable way, the level set method has a wide range of successful applications, including problems in fluid mechanics, combustion, solids modeling, computer animation, material science and image processing over the years [2–6].

Recently, the level set methods have been applied to structural shape and topology optimization problems as an emerging and promising family of methods based on the moving free boundaries [7–10]. Sethian and Wiegmann [7] are among the first researchers to extend the level set method of Osher and Sethian in [1] to capture the free boundary of a structure on a fixed Eulerian mesh. The Von Mises equivalent stress, rather than the more suitable classical shape sensitivity analysis, was employed to improve the structural rigidity within the context of two-dimensional linear elasticity using the immersed interface method. Osher and Santosa [11] investigated a two-phase optimization of a membrane modeled by a linear scalar partial differential equation. The free boundary was defined as the interface between two constituents occupying a given design domain. The level set method was combined with the shape sensitivity analysis framework, but without the context of linear or nonlinear elasticity. Wang et al. [9] established the speed (or velocity) vector in terms of the shape of the boundary and the variational sensitivity as a physically meaningful link between the general structural topology optimization process and the powerful level set methods. It was suggested that using the level set methods for structural topology optimization has the promising potentials in flexibility of handling topological changes, fidelity of boundary representation and degree of automation. The level set methods were further developed as a natural setting to combine the rigorous shape variations into the conventional structural topology optimization process in [10]. Allaire et al. [8] also proposed an implementation of the level-set methods for structural topology optimization where the front velocity during the optimization process was derived from the classical shape sensitivity analysis by using an adjoint problem and the front propagation was performed by solving the Hamilton–Jacobi equation. Furthermore, drastic topology changes during the structural optimization process were allowed for. In a multi-material design domain, the conventional level set methods have been further developed in [12] as a ''color level set'' method to address the problem of structural shape and topology optimization. An implicit function vector was used to represent different material phases more efficiently. It was demonstrated that the proposed method can automatically avoid the problem of overlap between material phases of a conventional partitioning approach. In [13], the conventional level set methods were further extended to a level set-based variational approach for the optimal shape and topology design of heterogeneous objects using a multi-phase level set model in [14] for digital image processing, in which the promising features such as strong regularity in the problem formulation and inherent capabilities of geometric and materials modeling have been obtained and illustrated. More recently, Xia et al. [15] presented a semi-Lagrangian method for level-set based shape and topology optimization. The level set Hamilton–Jacobi equation was solved by an efficient and unconditionally stable semi-Lagrange scheme and it was reported that a much larger time step size could be used to save the computational time significantly. Wang and Wang [16] explored the use of radial basis functions for the level set-based structural topology optimization. Multiquadric (MQ) splines were used to define the implicit function and some appealing results illustrated. However, a thorough investigation into the level set-based shape and topology optimization using the radial basis functions was not performed. Moreover, only the relatively simple unconstrained topology optimization with a fixed Lagrange multiplier, rather than the practical constrained shape and topology optimization with a variational Lagrange multiplier, was implemented.

The advantages of the level set methods as capturing methods based on embedding the interface as the zero-level set of a higher-dimensional function are well known. Generally, the level set methods provide a smooth geometrical description of the interface and require a relatively simple implementation and their extension to three-dimensional (3D) problems is straightforward [17,18]. In practice, in applying a level set model for structural shape and topology optimization, it should be noted that the implementation of the conventional discrete level set methods requires appropriate choice of the upwind schemes, extension velocities and reinitialization algorithms [16], where complicated PDE (partial differential equation) solving procedures are usually involved [2–4,9,12,19]. In general, it is well known that the PDEs are rarely easy to implement [20], though some robust and accurate methods such as the upwind schemes [1,21,22], fast marching methods [2] and fast local level set methods [17,18] have been available. Particularly, in solving the structural shape and topology optimization problems, the conventional level set methods [9,11,12,19,23] is known to be slow to reach the convergence and easy to get stuck at a local minimum [24]. Furthermore, there is no nucleation mechanism in the conventional level set methods, leading to the final design largely dependent on the initial guesses [2,6,16,25,26].

Although some attempts have been made to incorporate both the topological derivatives and the shape derivatives into a level set model to resolve this problem [25,26], it is shown to be difficult to switch between the topological derivatives and the shape derivatives [25,27,28]. Hence, the numerical considerations of discrete computation would severely limit the primary advantages of the conventional level set methods for structural shape and topology optimization.

The objective of the present study is to develop an alternative level set method with improved efficiency for structural shape and topology optimization by introducing the popular radial basis functions [29]. The implicit level set function is approximated by using the RBF implicit modeling with MQ splines [30]. The original Hamilton–Jacobi PDE is discretized into a mathematically more convenient system of ODEs and the original time dependent initial value problem becomes an interpolation problem for the initial values of the generalized expansion coefficients, which can be solved by a collocation formulation of the method of lines [31]. Due to the use of MQ RBFs with global support [30], a relatively smooth level set evolution can be maintained without reinitialization. A practical implementation of the present method is further developed, in which inaccurate solution to the original Hamilton–Jacobi PDE may be justified and nucleation of new holes inside the material domain is allowed for. As a result, the constraints on the temporal and spatial discretizations can be relaxed and the direct consequence of time stability problem can be circumvented and a rapid convergence to the final design insensitive to initial guesses becomes possible. The normal velocities are chosen to perform the steepest gradient-based shape and topology optimization by using shape sensitivity analysis [16,19,26] and a bi-sectioning algorithm [32]. An "ersatz material" approach [19] is used to perform the finite element analysis to obtain the strain energy density field and a bi-sectioning algorithm is proposed to find the Lagrange multiplier to ensure that the optimization process is performed in the feasible domain. The extension velocities are obtained by using the strain energy density field in the whole design domain and a linear smoothing filter [33] is used to smooth out the discontinuities at the free boundary. Numerical examples are chosen to illustrate the success of the present method in accuracy, convergence speed and insensitivity to initial designs in shape and topology optimization of 2D problems that has been extensively studied in the literature [9,16,19,23,25,34–36].

In the following, we first present an overview on the conventional level set methods. We then introduce the RBF implicit modeling for the implicit level set function. A RBF expansion coefficients-based governing equation of motion of the moving free boundary is then presented, followed by an application to classical shape and topology optimization. Numerical examples are discussed next with a comparative study on the efficiency and accuracy of the present method. The conclusions are finally given.

2. Conventional level set methods

Level set methods first devised by Osher and Sethian [1] have become popular recently for tracking, modeling and simulating the motion of dynamic interfaces (moving free boundaries) in fluid mechanics, combustion, computer animation, material science, crack propagation and image processing [2,4]. The interface (or front) is closed, nonintersecting and Lipschitz-continuous and represented implicitly through a Lipschitz-continuous level set function $\Phi(\mathbf{x})$, and the interface itself is the zero isosurface or zero level set $\{\mathbf{x} \in \mathbb{R}^d | \Phi(\mathbf{x}) = 0\}$ ($d = 2$ or 3). The embedding $\Phi(\mathbf{x})$ of $(d+1)$ dimension can be specified in any specific form, such as a regular sampling on a rectilinear grid. Furthermore, $\Phi(\mathbf{x})$ can be used to define the inside and outside regions of the interface as follows:

$$\begin{aligned} &\Phi(\mathbf{x}) = 0 \quad \forall \mathbf{x} \in \partial\Omega \cap D, \\ &\Phi(\mathbf{x}) < 0 \quad \forall \mathbf{x} \in \Omega \setminus \partial\Omega, \\ &\Phi(\mathbf{x}) > 0 \quad \forall \mathbf{x} \in (D \setminus \Omega), \end{aligned} \tag{1}$$

where $D \subset \mathbb{R}^d$ is a fixed design domain in which all admissible shapes Ω (a smooth bounded open set) are included, i.e. $\Omega \subset D$. The local unit normal to the surface n can be given by

$$n = \frac{\nabla\Phi}{|\nabla\Phi|} \quad (\text{where } |\nabla\Phi| = \sqrt{\nabla\Phi \cdot \nabla\Phi}). \tag{2}$$

In the level set methods, it is convenient to use the Heaviside step function H and the Dirac delta function δ defined [9,37] as

$$H(\Phi) = \begin{cases} 1, & \Phi \geqslant 0, \\ 0, & \Phi < 0, \end{cases} \quad \delta(\Phi) = H'(\Phi), \quad \delta(\mathbf{x}) = \nabla H \cdot \frac{\nabla \Phi}{|\nabla \Phi|} = \delta(\Phi)|\nabla \Phi|. \tag{3}$$

Then, the interior and the boundary Γ of a shape can be described in terms of the level set function $\Phi(\mathbf{x})$, respectively, as

$$\Omega = \{\mathbf{x} : H(-\Phi(\mathbf{x})) = 1\}, \quad \Gamma = \{\mathbf{x} : \delta(\Phi(\mathbf{x})) > 0\}. \tag{4}$$

Furthermore, in the level set formulation, the volume integral of a function $F(\mathbf{x})$ is defined as

$$\int_{\mathrm{D}} F(\mathbf{x}) H(-\Phi)\, \mathrm{d}\Omega.$$

If $F(\mathbf{x}) \equiv 1$, then this integral yields the volume $V(\Phi)$ as follows:

$$V(\Phi) = \int_{\mathrm{D}} H(-\Phi)\, \mathrm{d}\Omega. \tag{5}$$

To let the level set function dynamically change in time, a continuous velocity field v, which is a function of position $\mathbf{x}$, is introduced and the evolution can be described as the following Cauchy problem [6]:

$$\frac{\partial \Phi}{\partial t} + v \cdot \nabla \Phi = 0, \quad \Phi(\mathbf{x}, 0) = \Phi_0(\mathbf{x}), \tag{6}$$

where $\Phi_0(\mathbf{x})$ embeds the initial position of the interface and t the artificial time. According to Eq. (2), (6) can be re-written using the normal velocity v_{n} as

$$\frac{\partial \Phi}{\partial t} + v_n |\nabla \Phi| = 0, \quad \Phi(\mathbf{x}, 0) = \Phi_0(\mathbf{x}), \tag{7}$$

where

$$v_n = v \cdot \frac{\nabla \Phi}{|\nabla \Phi|}. \tag{8}$$

In the conventional level set methods, the Hamilton–Jacobi PDE (7) is solved to evolve the interface using a capturing Eulerian approach. The solving procedure requires appropriate choice of the upwind schemes, reinitialization algorithms and extension velocity methods, which may require excessive amount of computational efforts and thus limit the utility of the level set methods. Moreover, the Hamilton–Jacobi PDE (7) obeys a maximum principle [4] and thus the nucleation of holes inside the material domain is prohibited. Hence, the final design becomes strongly dependent on the initial guess which decides the maximum number of holes allowed [2,9,19,26].

In the present study, an extended level set method for shape and topology optimization is proposed based on a modification of the conventional level set methods. The benefits of handling topological changes of the implicit representation of a level set model are retained while the implicit level set function is to be approximated by an implicit modeling method based on radial basis functions to achieve the global smoothness. Parametrization of the RBF implicit model discretizes the Hamilton–Jacobi PDE into a system of mathematically more convenient coupled ODEs. Moreover, reinitialization becomes unnecessary because of the global approximation. By imposing an approximation method in solving the coupled ODEs, the objective function value can still be decreased while the constraint conditions satisfied. The limits on the total number of knots and the timestep size can be relaxed and the computational efficiency can be improved. More importantly, the nucleation of new holes is thus allowed for. This proposed method is to be discussed in detail in the following sections.

3. Extended level set method using an implicit RBF modeling

3.1. RBF implicit modeling for the level set function

To model and reconstruct the entire admissible design with a single level set function which is globally continuous and differentiable, an implicit modeling method based on RBFs is presented. RBFs are popular for

interpolating scattered data to produce smooth surface/boundary as the associated system of non-linear equations is guaranteed to be invertible under mild conditions on the locations of the data points [38]. The positive features of radial basis functions such as the unique solvability of the interpolation problem, the computation of interpolants, their smoothness and convergence make them very attractive in the level set methods. In the present study, RBF implicit modeling is to be presented as an effective representation method to reconstruct the moving free boundary via the implicit level set function.

Radial basis functions are radially-symmetric functions centered at a particular point [39], or knot, which can be expressed as follows:

$$\varphi_i(\mathbf{x}) = \varphi(\|\mathbf{x} - \mathbf{x}_i\|), \quad \mathbf{x}_i \in D, \tag{9}$$

where $\|\cdot\|$ denotes the Euclidean norm on $\mathbb{R}^d$ [30], and $\mathbf{x}_i$ the position of the knot. Only a single fixed function form $\varphi : \mathbb{R}^+ \to \mathbb{R}$ with $\varphi(0) \geqslant 0$ is used as the basis to form a family of independent functions. There is a large class of possible radial basis functions. Commonly used RBFs include thin-plate spline, polyharmonic splines, Sobolev splines, Gaussians, multiquadrics and compactly supported RBFs [30,31]. Among them, the multiquadric (MQ) spline appears to be the overall best performing RBF [30], which can be written as

$$\varphi_i(\mathbf{x}) = \sqrt{(\mathbf{x} - \mathbf{x}_i)^2 + c_i^2}, \tag{10}$$

where c_i is the free shape parameter which is commonly assumed to be a constant for all i in most applications. It should be noted that $\varphi_i(\mathbf{x})$ in Eq. (10) is continuously differentiable and thus MQ splines are infinitely smooth splines [31].

In the present RBF implicit modeling, the MQ spline is used to interpolate the scalar implicit level set function $\Phi(\mathbf{x})$ with N knots by using N MQs centered at these knots. The resulting RBF interpolant of the implicit function can be written as

$$\Phi(\mathbf{x}) = \sum_{i=1}^{N} \alpha_i \varphi_i(\mathbf{x}) + p(\mathbf{x}), \tag{11}$$

where α_i is the weight, or expansion coefficient, of the radial basis function positioned at the ith knot, $p(\mathbf{x})$ a first-degree polynomial to account for the linear and constant portions of $\Phi(\mathbf{x})$ and to ensure positive definiteness of the solution [39]. For the three-dimensional (3D) modeling problems, $p(\mathbf{x})$ can be given by

$$p(\mathbf{x}) = p_0 + p_1 x + p_2 y + p_3 z \tag{12}$$

in which p_0, p_1, p_2 and p_3 are the coefficients of the polynomial $p(\mathbf{x})$. Because of the introduction of this polynomial, to ensure a unique solution, the RBF interpolant of $\Phi(\mathbf{x})$ in Eq. (11) must be subject to the following side constraints [31,38–40]:

$$\sum_{i=1}^{N} \alpha_i = 0, \quad \sum_{i=1}^{N} \alpha_i x_i = 0, \quad \sum_{i=1}^{N} \alpha_i y_i = 0, \quad \sum_{i=1}^{N} \alpha_i z_i = 0. \tag{13}$$

If the interpolation data values $f_1, \ldots, f_N \in \mathbb{R}$ at knot locations $\mathbf{x}_1, \ldots, \mathbf{x}_N \in D \subset \mathbb{R}^d$ are given, the RBF interpolant of $\Phi(\mathbf{x})$ in Eq. (11) can be obtained by solving the system of $N + 4$ linear equations for $N + 4$ unknown generalized expansion coefficients:

$$\begin{aligned} &\Phi(\mathbf{x}_i) = f_i, \quad i = 1, \ldots, N, \\ &\sum_{i=1}^{N} \alpha_i = 0, \quad \sum_{i=1}^{N} \alpha_i x_i = 0, \quad \sum_{i=1}^{N} \alpha_i y_i = 0, \quad \sum_{i=1}^{N} \alpha_i z_i = 0 \end{aligned} \tag{14}$$

which can be re-written in matrix form as

$$\mathbf{H}\boldsymbol{\alpha} = \mathbf{f}, \tag{15}$$

where

$$\mathbf{H} = \begin{bmatrix} \mathbf{A} & \mathbf{P} \\ \mathbf{P}^{\mathrm{T}} & \mathbf{0} \end{bmatrix} \in \mathbb{R}^{(N+4)\times(N+4)}, \tag{16}$$

$$\mathbf{A} = \begin{bmatrix} \varphi_1(\mathbf{x}_1) & \cdots & \varphi_N(\mathbf{x}_1) \\ \vdots & \ddots & \vdots \\ \varphi_1(\mathbf{x}_N) & \cdots & \varphi_N(\mathbf{x}_N) \end{bmatrix} \in \mathbb{R}^{N\times N}, \tag{17}$$

$$\mathbf{P} = \begin{bmatrix} 1 & x_1 & y_1 & z_1 \\ \vdots & \vdots & \vdots & \vdots \\ 1 & x_N & y_N & z_N \end{bmatrix} \in \mathbb{R}^{N\times 4}, \tag{18}$$

$$\boldsymbol{\alpha} = [\,\alpha_1 \quad \cdots \quad \alpha_N \quad p_0 \quad p_1 \quad p_2 \quad p_3\,]^{\mathrm{T}} \in \mathbb{R}^{N+4}, \tag{19}$$

$$\mathbf{f} = [\,f_1 \quad \cdots \quad f_N \quad 0 \quad 0 \quad 0 \quad 0\,]^{\mathrm{T}} \in \mathbb{R}^{N+4}. \tag{20}$$

Since the multiquadric collocation matrix $\mathbf{H}$ is theoretically invertible [29,31,41], the generalized expansion coefficients $\boldsymbol{\alpha}$ can be simply given by

$$\boldsymbol{\alpha} = \mathbf{H}^{-1}\mathbf{f}. \tag{21}$$

After obtaining the generalized expansion coefficients $\boldsymbol{\alpha}$, the resulting RBF interpolant of the implicit function in Eq. (11) can be re-written compactly as

$$\Phi(\mathbf{x}) = \boldsymbol{\phi}^{\mathrm{T}}(\mathbf{x})\boldsymbol{\alpha}, \tag{22}$$

where

$$\boldsymbol{\phi}(\mathbf{x}) = [\,\varphi_1(\mathbf{x}) \quad \cdots \quad \varphi_N(\mathbf{x}) \quad 1 \quad x \quad y \quad z\,]^{\mathrm{T}} \in \mathbb{R}^{(N+4)\times 1}. \tag{23}$$

It should be noted that the system of the form (15)–(20) is a special case of the more general saddle point systems (or KKT systems in the optimization literature) [42]. Hence, the solution methods reviewed in detail in [42] for generalized saddle point problems are applicable to efficiently solve this system, such as the direct solvers, stationary iterative methods, Krylov subspace solvers, preconditioners, multigrid and Schwarz-type algorithms.

3.2. Governing equation of motion

Since the Hamilton–Jacobi PDE (7) is time dependent, in the present RBF implicit modeling for the level set function $\Phi(\mathbf{x})$, it is further assumed that all the knots are fixed in space and the space and time are separable and the time dependence of the implicit function Φ is due to the generalized expansion coefficients $\boldsymbol{\alpha}$ of the RBF interpolant in Eq. (19). With these assumptions, the RBF interpolant of the implicit function in Eq. (22) becomes time dependent as

$$\Phi = \Phi(\mathbf{x}, t) = \boldsymbol{\phi}^{\mathrm{T}}(\mathbf{x})\boldsymbol{\alpha}(t). \tag{24}$$

Substituting Eq. (24) into the Hamilton–Jacobi PDE defined in (7) yields

$$\boldsymbol{\phi}^{\mathrm{T}}\frac{\mathrm{d}\boldsymbol{\alpha}}{\mathrm{d}t} + v_n|(\nabla\boldsymbol{\phi})^{\mathrm{T}}\boldsymbol{\alpha}| = 0, \tag{25}$$

where

$$|(\nabla\boldsymbol{\phi})^{\mathrm{T}}\boldsymbol{\alpha}| = \left[\left(\frac{\partial\boldsymbol{\phi}^{\mathrm{T}}}{\partial x}\boldsymbol{\alpha}\right)^2 + \left(\frac{\partial\boldsymbol{\phi}^{\mathrm{T}}}{\partial y}\boldsymbol{\alpha}\right)^2 + \left(\frac{\partial\boldsymbol{\phi}^{\mathrm{T}}}{\partial z}\boldsymbol{\alpha}\right)^2\right]^{1/2}, \tag{26}$$

$$\frac{\partial\boldsymbol{\phi}}{\partial x} = \left[\frac{\partial\varphi_1}{\partial x} \quad \cdots \quad \frac{\partial\varphi_N}{\partial x} \quad 0 \quad 1 \quad 0 \quad 0\right]^{\mathrm{T}} \in \mathbb{R}^{(N+4)\times 1}, \tag{27}$$

$$\frac{\partial\boldsymbol{\phi}}{\partial y} = \left[\frac{\partial\varphi_1}{\partial y} \quad \cdots \quad \frac{\partial\varphi_N}{\partial y} \quad 0 \quad 0 \quad 1 \quad 0\right]^{\mathrm{T}} \in \mathbb{R}^{(N+4)\times 1}, \tag{28}$$

$$\frac{\partial\boldsymbol{\phi}}{\partial z} = \left[\frac{\partial\varphi_1}{\partial z} \quad \cdots \quad \frac{\partial\varphi_N}{\partial z} \quad 0 \quad 0 \quad 0 \quad 1\right]^{\mathrm{T}} \in \mathbb{R}^{(N+4)\times 1}, \tag{29}$$

$$\frac{\partial \varphi_i}{\partial x} = \frac{x - x_i}{\sqrt{(x-x_i)^2 + (y-y_i)^2 + (z-z_i)^2 + c_i^2}}, \quad i = 1, \ldots, N, \tag{30}$$

$$\frac{\partial \varphi_i}{\partial y} = \frac{y - y_i}{\sqrt{(x-x_i)^2 + (y-y_i)^2 + (z-z_i)^2 + c_i^2}}, \quad i = 1, \ldots, N, \tag{31}$$

$$\frac{\partial \varphi_i}{\partial z} = \frac{z - z_i}{\sqrt{(x-x_i)^2 + (y-y_i)^2 + (z-z_i)^2 + c_i^2}}, \quad i = 1, \ldots, N. \tag{32}$$

In Eq. (25), the RBF expansion coefficients are explicitly time dependent and all the time dependence is due to the expansion coefficients. At the initial time, all the time dependent variables should be specified over the entire domain. This initial value problem can be considered equivalent to an interpolation problem since the expansion coefficients at the initial time are found as a solution of the interpolation problem, as shown in Eq. (15). Hence, the preliminary starting point of the use of RBFs to solve PDEs is the interpolation problem that is equivalent to solving the initial value problem. The original time-dependent initial value problem defined by the Hamilton–Jacobi PDE (7) in the conventional level set methods is thus converted into a time-dependent interpolation problem for the initial values of the generalized expansion coefficients $\boldsymbol{\alpha}$ and the motion of the free boundary, or the propagation of the front, is now governed by the time dependent coupled equation (25).

To time advance the initial values of $\boldsymbol{\alpha}$ in the governing equation of motion (25), a collocation formulation of the method of lines is presented because of its inherent simplicity. The governing equation of motion of the front equation (25) is extended to the whole design domain D and the normal velocities v_n at the front are thus replaced by the extension velocities v_n^e in D. Based on the principle of collocation method, all nodes of the spatial discretization of the extended ODE (25) are located sequentially at the fixed knots of the RBF interpolation for the implicit function $\Phi(\mathbf{x})$. Furthermore, in the present implementation, for the purpose of simplicity, all the nodes of a fixed mesh for structural analysis are taken as the fixed knots of RBF interpolation, though not necessary. However, using this collocation method cannot guarantee the positive definiteness of the resulting system due to the conditional positive definiteness of the multiquadrics [31,43]. Similar to solving the interpolation problem using RBFs in Eq. (14), side constraints must be introduced to guarantee that the generalized coefficients $\boldsymbol{\alpha}$ can be solved. For this time-dependent interpolation problem, the corresponding side constraints are proposed as follows:

$$\sum_{i=1}^{N} \dot{\alpha}_i(t) = 0, \quad \sum_{i=1}^{N} \dot{\alpha}_i(t) x_i = 0, \quad \sum_{i=1}^{N} \dot{\alpha}_i(t) y_i = 0, \quad \sum_{i=1}^{N} \dot{\alpha}_i(t) z_i = 0. \tag{33}$$

Using the present collocation method for the N knots and the four side constraints in (33), a set of resulting ODEs can be compactly written as follows:

$$\mathbf{H}\frac{\mathrm{d}\boldsymbol{\alpha}}{\mathrm{d}t} + \mathbf{B}(\boldsymbol{\alpha}) = 0, \tag{34}$$

where

$$\mathbf{B}(\boldsymbol{\alpha}) = \begin{bmatrix} v_n^e(\mathbf{x}_1)|(\nabla \boldsymbol{\phi}^T(\mathbf{x}_1))\boldsymbol{\alpha}| \\ \vdots \\ v_n^e(\mathbf{x}_N)|(\nabla \boldsymbol{\phi}^T(\mathbf{x}_N))\boldsymbol{\alpha}| \\ 0 \\ 0 \\ 0 \\ 0 \end{bmatrix} \in \mathbb{R}^{(N+4)\times 1}. \tag{35}$$

It should be noted that the same collocation matrix $\mathbf{H}$ as Eq. (15) has been derived because of the proposed side constraints in (33). Since the collocation matrix $\mathbf{H}$ is theoretically invertible as aforementioned, the resulting

ODE system in (34) is solvable and nonsingular. Eq. (34) can be regarded as a collocation formulation of the general method of lines [44], in which a time dependent PDE problem is reduced to a simpler time dependent ODE problem by discretization. The method of lines has a solid mathematical foundation and the convergence of the solution of the converted ODE problem to the solution of the original PDE problem has been rigorously proven [44].

It is well known that in many situations the level set function may develop flat and/or steep gradients leading to problems in numerical approximations using the local approximation methods such as the upwind schemes [6,17]. To cope with these problems, a reinitialization procedure is periodically performed to resurrect the behavior of the level set function in the neighborhood of the front, while keeping the zero location unchanged. In the present global approximation method using RBF implicit modeling for the level set function, the occurrence of flat level set function in the neighborhood of the front is virtually prevented due to the explicit parametrization of the RBF implicit model. The parametrization with global support makes the level set function and its gradients at any point dependent on each knot value in the whole design domain, rather than the neighboring knot values only, different from the upwind schemes [4]. According to Eqs. (26)–(32), during the course of evolution it can be generally maintained that

$$|\nabla \Phi| = |(\nabla \boldsymbol{\phi})^{\mathrm{T}} \boldsymbol{\alpha}| \neq 0 \tag{36}$$

for most points in the neighborhood of the front $\Phi = \boldsymbol{\phi}^{\mathrm{T}}\boldsymbol{\alpha} = 0$ and thus a flat surface is unlikely to be developed. Hence, a smooth level set evolution can thus be achieved. In our numerical examples, it has never been experienced that $|\nabla\Phi| = 0$ when $\Phi = 0$. It should be noted that in the literature [45] using non-local functionals was reported to obtain almost smooth level set evolution through a regularization method without reinitialization, though radial basis functions were not considered. Furthermore, since the gradients can be readily obtained from (26) to (32), steep gradients will not lead to the apparent numerical approximation problems existing in the local approximation methods such as the upwind schemes [4]. Moreover, the magnitude of the gradients can be scaled down since the generalized expansion coefficients $\boldsymbol{\alpha}$ can be normalized without changing the zero location $\Phi(\mathbf{x}) = 0$, according to the present RBF approximation (22) for the implicit level set function. Hence, reinitialization becomes unnecessary and can be eliminated in the numerical analysis procedure in solving the coupled ODEs (34). It should be noted that in the recent literature, many level set methods without reinitialization have been proposed, as seen in [24,45–48]. In the present study, the global basis functions are used to prevent the concurrence of flat level sets and to maintain the behavior of the level set function at the front without reinitialization.

The set of coupled non-linear ODEs of Eq. (34) can be solved by several well-established ODE solvers such as the first-order forward Euler's method and higher-order Runge–Kutta, Runge–Kutta–Fehlberg, Adams–Bashforth, or Adams–Moulton methods [49]. In the present study, only the first-order forward Euler's method is used since it is the simplest solution algorithm for ODE initial condition problems and often used for comparison with more accurate algorithms, which are more complex and tedious to implement. Using Euler's method, an approximate solution to Eq. (34) can be given by

$$\boldsymbol{\alpha}(t^{n+1}) = \boldsymbol{\alpha}(t^{n}) - \tau \mathbf{H}^{-1}\mathbf{B}(\boldsymbol{\alpha}(t^{n})), \tag{37}$$

where τ is the timestep size. Because of the fixed location of the RBF knots, the multiquadric collocation matrix $\mathbf{H}$ is time independent and storing the initial value of its inverse matrix only will save the computational cost. The use of the time independent collocation matrix and its inverse matrix may still be a drawback of the present method in computational efficiency due to the problem size, compared with the popular upwind schemes [4]. However, this drawback can be significantly alleviated when the present extended level set method is applied to shape and topology optimization problems. Usually, the timestep size should be sufficiently small to achieve the numerical stability due to the Courant–Friedrichs–Lewy (CFL) condition for stability in the von Neumann sense [4]. Furthermore, the truncation error due to the spatial discretization of the implicit RBF modeling should be kept small enough. A small timestep size together with a large number of RBF knots can be used to achieve an accurate solution to the original Hamilton–Jacobi PDE, however, the computational time will be increased significantly and the computational efficiency may pose a severe problem. To improve the computational efficiency, in the present extended level set method for shape and topology optimization, only an approximate solution to the Hamilton–Jacobi PDE is pursued such that the constraints on the timestep size

τ and the total number of RBF knots N can be significantly relaxed and nucleation of new holes can be allowed for. A detailed discussion is to be given in the following section.

3.3. Practical implementation of the extended level set method

As noted by many researchers [6,48,50–52], a wide range of practical problems can be expressed in variational form as follows:

$$\begin{aligned} &\underset{\Phi}{\text{Minimize}} \quad J(\mathbf{u},\Phi) = \int_D F(\mathbf{u})H(-\Phi)\,\mathrm{d}\Omega \\ &\text{subject to :} \quad G(\mathbf{u},\Phi) = \int_D g(\mathbf{u})H(-\Phi)\,\mathrm{d}\Omega = 0, \end{aligned} \tag{38}$$

where J is an energy functional, F the energy density, $\mathbf{u}$ a field variable, G a constraint functional, g a constraint function. It is well known that the level set methods can be used to solve this kind of optimization problems provided that both J and G are Gâteaux-differentiable functionals and the corresponding methods are called variational level set methods [6,48,50–52]. Based on the normal velocities derived from the steepest descent method and the shape derivatives, the moving free boundary can be captured by solving the Hamilton–Jacobi equations (6) or (7) and an optimal solution to (38) can be finally obtained. Ideally, if both J and G are convex, this optimal solution is also the global minimum and independent of the initial guess [53]. However, in most cases using the variational level set methods [6,16,23,48,50–52], neither J nor G can be convex. Hence, the final optimal solution obtained by the conventional gradient-based variational level set methods largely depends on the initial guess [19]. This dependency may even make the optimization solution procedure fail to converge if a bad guess is chosen [24]. It was observed by many researchers [9,19,25,26] that each optimal solution cannot have more holes than the geometry of the initial guess due to the lack of a nucleation mechanism in the conventional level set methods [6]. Hence, the global optimum can never be reached if it has more holes than the initial geometry. One common approach in getting around this problem is to initially seed many small holes that are densely distributed throughout the given design domain and let them gradually merge and evolve [6]. However, this approach may become less practical since the gradient-based local search method may easily get stuck at a local minimum [53–55] considering the fact that the original optimization problem (38) usually has one global optimum and many local minima. Due to the theoretical complexity and computational cost in locating the global optimum, for many real world problems, the global optimum is only of theoretical importance. It is practically more useful to derive a local optimal solution less sensitive to the initial guess since the local minima problem can be relieved without increasing the computational cost significantly.

In the literature, many efforts have been made to find a local optimal solution to (38) less sensitive to the initial guess. In the work of Chan and Vese [56], particular choice of a delta function that has non-compact support was proposed to replace $|\nabla\Phi|$ in the Hamilton–Jacobi equation (7). It was reported that new interior contour my occur due to this special handling on the Hamilton–Jacobi PDE and thus the final geometry will become less dependent of the initial configuration. However, more careful study is needed to compare the degree of regularization with the possibility of the emergence of new interior contour since the continuity of the level set function is discarded [6]. In the work of Burger et al. [26], a forcing term dependent on the topological derivative was added to modify the Hamilton–Jacobi equation (7). Although the limited capability of the standard shape derivative based level set method to generate holes can be improved due to this modification, it is shown to be difficult to switch between the topological derivatives and the shape derivatives. In the work of Allaire et al. [25], the standard level set method based on the classical shape derivative was coupled with the topological gradient method for introducing new holes in the optimization process. It was reported that this coupling can escape from local minima in a given topological class of shapes. However, it was also shown that incorporating the topological derivatives is quite difficult in numerical practice since a hole can not be smaller than a single mesh cell and thus cannot be infinitesimally small as defined by the topological derivatives. It should also be noted that in Haber's recent work [24] the level set method was used to represent the shape, but the Hamilton–Jacobi equations were avoided all together and the shape optimization problem was treated as a numerical optimization problem only using

a reduced Hessian Sequential Quadratic Programming (SQP) method combined with multilevel continuation techniques. It was reported that the optimization problem can be solved rapidly compared with the efficiency of the conventional level set methods. As a whole, in order to generate more efficient optimal solutions less sensitive to the initial guess, some perturbations or modifications of the conventional level set methods must be introduced.

In the present extended level set method, relatively simple modifications of the conventional level set methods are proposed to generate optimal designs insensitive to the initial guess. The choice of the timestep size τ and the total number of RBF knots N are determined by decreasing the energy functional J while remaining in the feasible region, rather than by solving the Hamilton–Jacobi PDE accurately. This modification will lead to an inaccurate solution to the standard Hamilton–Jacobi PDE, similar to those modifications of the Hamilton–Jacobi PDE previously discussed [25,26,56]. The maximum principle [4] will not be strictly satisfied and therefore nucleation of new holes inside the material domain becomes possible. Hence, the final design can become less strongly dependent on the initial guess and the computational efficiency in solving the optimization problem (38) can be improved, as demonstrated in the present numerical examples. It is well known that the conventional level set methods can only solve the optimization problem (38) quite inefficiently [24] since the convergence speed is usually slow and the probability to converge to a local minimum is high. In many situations, timestep sizes are not chosen to satisfy the accuracy requirements or to achieve a rapid convergence but rather to satisfy the CFL condition for stability, resulting in a loss of computational efficiency. In the present method, since the the timestep size τ and the total number of RBF knots N are chosen to satisfy the optimization requirements only, both temporal and spatial discretizations are less severely restricted and thus a faster convergence speed can be obtained. Without satisfying the CFL condition for stability explicitly, the present method can still maintain a relatively smooth evolution of the level set function without reinitialization, as aforementioned. Furthermore, since the generalized expansion coefficients $\boldsymbol{\alpha}$ can be normalized without changing the zero location $\Phi(\mathbf{x}) = 0$, the magnitude of the level set function can be kept bounded and thus the direct consequence of time stability problem caused by the present modifications can be circumvented and would become negligible.

Hence, a practical implementation of the present extended level set method for the optimization problem (38) is developed. The implicit level set function is used to handle significant topological changes readily, while the disadvantages of conventional level set methods in solving a local optimization problem efficiently and requiring a periodic reinitialization process are overcome. This implementation is finally applied to the classical shape and topology optimization problems to demonstrate its success in accuracy and efficiency.

4. Shape and topology optimization using the level set method

The classical shape and topology optimization problem is chosen as an application of the present extended level set method. The proposed shape and topology optimization process operates on the implicit scalar level set function $\Phi(\mathbf{x})$ defined in Eq. (1) and represented by the RBF implicit modeling in (22) and uses a steepest gradient method to find the decent direction of the normal velocity for the minimization of an objective function $J(\Phi)$. The normal velocity at the front is naturally and smoothly extended to the whole design domain D without using any additional PDE solving procedure.

4.1. Minimum compliance design

In the classical shape and topology optimization problems, the minimum compliance design has been widely investigated by the popular topology optimization methods such as the homogenization method [57] and the evolutionary structural optimization method [35]. It should be noted that, as an important alternative approach to the homogenization method, the SIMP (solid isotropic microstructure with penalization) method [58] originally introduced by Bendsøe [59], has been generally accepted in recent years [55,60,61].

With a level set model as shown in Eq. (1), the standard notion [33] of a classical minimum compliance design problem can be re-written as follows:

$$\begin{aligned} &\underset{\Phi}{\text{Minimize}} \quad J(\mathbf{u},\Phi) = \int_D (\boldsymbol{\varepsilon}(\mathbf{u}))^{\mathrm{T}}\mathbf{C}\boldsymbol{\varepsilon}(\mathbf{u})H(-\Phi)\,\mathrm{d}\Omega \\ &\text{subject to}: \quad a(\mathbf{u},\upsilon,\Phi) = L(\upsilon,\Phi), \quad \mathbf{u}|_{\Gamma_{\mathrm{D}}} = \mathbf{u}_0, \quad \forall \upsilon \in U, \\ &\qquad\qquad V(\Phi)/V_0 = \zeta, \end{aligned} \tag{39}$$

where $J(\mathbf{u},\Phi)$ is the objective function, $\mathbf{u}$ the displacement field, $\boldsymbol{\varepsilon}(\mathbf{u})$ the strain field, $\mathbf{C}$ the Hook elasticity tensor, $V(\Phi)$ the material volume as defined in Eq. (5), V_0 the design domain volume and ζ the prescribed volume fraction. The linearly elastic equilibrium equation is written in its weak variational form in terms of the energy bilinear form $a(\mathbf{u},\upsilon,\Phi)$ and the load linear form $L(\upsilon,\Phi)$ [33], with υ denoting a virtual displacement field in the space U of kinematically admissible displacement fields, and $\mathbf{u}_0$ the prescribed displacement on the admissible Dirichlet boundary Γ_{D}.

The Lagrange multiplier method can be used to solve the optimization problem (39) [11]. By setting the constraint on the equilibrium state inactive, the Lagrangian $\mathscr{L}(\mathbf{u},\Phi,\ell)$ with a positive Lagrange multiplier ℓ can be given by

$$\mathscr{L}(\mathbf{u},\Phi,\ell) = J(\mathbf{u},\Phi) + \ell G(\Phi), \tag{40}$$

where the constraint functional $G(\Phi)$ can be expressed as

$$G(\Phi) = V(\Phi) - \zeta V_0 = 0. \tag{41}$$

It should be noted that the displacement field $\mathbf{u}$ is also a function of Φ, i.e. $\mathbf{u} = \mathbf{u}(\Phi)$. According to the Kuhn–Tucker condition of the optimization, the necessary condition for a minimizer is

$$D_\Phi \mathscr{L}(\mathbf{u}(\Phi),\Phi,\ell) = 0, \tag{42}$$

where $D_\Phi \mathscr{L}(\mathbf{u}(\Phi),\Phi,\ell)$ is the gradient of the Lagrangian with respect to Φ. Hence, both Φ and ℓ can be found by solving Eqs. (41) and (42).

4.2. Shape derivatives

The gradient of the Lagrangian $D_\Phi \mathscr{L}(\mathbf{u}(\Phi),\Phi,\ell)$ may be obtained in a number of different ways following the well-known approach of Murat and Simon of shape diffeomorphism [62]. In the present study, the shape sensitivity analysis presented by Allaire et al. [8] is adopted to derive the shape derivatives.

Usually, the boundary ∂D of the whole structural shape and topology design domain D can be decomposed [8] as

$$\partial D = \partial D_{\mathrm{D}} \cup \partial D_{\mathrm{N}} \cup \partial D_{\mathrm{H}}, \tag{43}$$

where ∂D_{D} is the Dirichlet boundary, ∂D_{N} the non-homogeneous Neumann boundary, and ∂D_{H} the homogeneous Neumann boundary (traction free). To derive the shape derivatives from the classical shape sensitivity analysis [62], it is assumed that the shape boundary $\partial\Omega$ of an admissible design Ω can satisfy the following conditions:

$$\partial\Omega = \Gamma_{\mathrm{D}} \cup \Gamma_{\mathrm{N}}, \quad \Gamma_{\mathrm{D}} \subset \partial D_{\mathrm{D}}, \quad \Gamma_{\mathrm{N}} = \partial D_{\mathrm{N}} \cup \Gamma_{\mathrm{H}}, \tag{44}$$

where Γ_{D} is the admissible Dirichlet boundary, Γ_{N} the Neumann boundary, and Γ_{H} the homogeneous Neumann boundary. Furthermore, it is assumed that the surface loads are design independent and applied only on a fixed subset of the boundary Γ_{N} and the Dirichlet boundary Γ_{D} is with zero displacements. The whole traction free homogeneous Neumann boundary Γ_{H} may be represented by the zero level set function. However, in the initial designs the strain energy density can be too high at the traction free boundary near the loading points at the non-homogeneous Neumann boundary or near the Dirichlet boundary due to the stress concentration, which may generate an undesirable maximum normal velocity in the early evolution as later discussed. Therefore, in the present shape and topology optimization, only part of the traction free homogeneous Neumann boundary $\Gamma_{\mathrm{M}} \in \Gamma_{\mathrm{H}}$ is initially chosen to be optimized as the moving free boundary, which is represented by the dynamic interface $\Phi(\mathbf{x}) = 0$ in the present level set model. It should also be noted that this handling will not prevent the whole boundary from being optimized due to the optimal time propagation of the moving free boundary.

Based on local perturbations of the moving free boundary of an admissible design Ω [8] (continuous perturbations with respect to the Hausdorff distance [26]), the resulting shape derivative of the Lagrangian can be written as

$$\frac{\mathrm{d}\mathscr{L}}{\mathrm{d}t} = \int_D (\ell - \boldsymbol{\varepsilon}^{\mathrm{T}}\mathbf{C}\boldsymbol{\varepsilon})\delta(\Phi)|\nabla\Phi|v_n \,\mathrm{d}\Omega \tag{45}$$

which can be further simplified [37] as

$$\frac{\mathrm{d}\mathscr{L}}{\mathrm{d}t} = \int_{\Gamma_{\mathrm{M}}} (\ell - \boldsymbol{\varepsilon}^{\mathrm{T}}\mathbf{C}\boldsymbol{\varepsilon})v_n \,\mathrm{d}s, \tag{46}$$

where t is the artificial time, and v_{n} the artificial normal velocity at the moving free boundary Γ_{M}. Furthermore, the resulting shape derivative of the volume constraint functional $G(\Phi)$ (41) can be expressed as

$$\frac{\mathrm{d}G}{\mathrm{d}t} = \int_{\Gamma_{\mathrm{M}}} v_n \,\mathrm{d}s. \tag{47}$$

Hence, these shape derivatives can be obtained from a surface integration. In a level set model, only the normal velocity field v_{n} is needed and thus it is unnecessary to perform an explicit surface integration. In the present shape and topology optimization, choosing the normal velocity field v_{n} is equivalent to choosing a descent direction for the objective function, which can be easily implemented by using a steepest gradient method [8,9,11].

4.3. Normal velocities

According to the shape derivative in Eq. (46), a descent direction of the normal velocity v_{n} for the Lagrangian can be obtained by simply identifying the normal velocity v_{n} as

$$v_n = \boldsymbol{\varepsilon}^{\mathrm{T}}\mathbf{C}\boldsymbol{\varepsilon} - \ell \tag{48}$$

in which the normal velocity v_{n} at the moving free boundary Γ_{M} can be determined by the strain energy density and a Lagrange multiplier. Hence, the normal velocity field is linked with the objective function of the present minimum compliance design problem and physics of the present problem is incorporated due to the flexibility of a level set model in choosing the velocity function. Without remeshing, the strain energy density field can be accurately and efficiently obtained numerically by using the "ersatz material" approach [8], the geometry projection method [63] or some extended finite element methods [23,64–66], though the standard finite element method without remeshing is not applicable due to the movement of the free boundary across the elements. However, the calculation of the Lagrange multiplier ℓ is not so straightforward.

To find the variable Lagrange multiplier ℓ, only several methods were available in the open literature, which appear to be less effective. In the work of Allaire et al. [8], as well as of Wang and Wang [16], a fixed ℓ was used during the evolution of the free boundary and thus the volume constraint cannot be satisfied and only an unconstrained optimization can be performed. The possible applications may become quite limited since the real-world optimization problems are usually constrained. In the work of Wang et al. [9], the variable Lagrange multiplier was derived from an assumption that the material volume keeps constant during the evolution such that its shape derivative defined in (47) vanishes. However, this handling may become even conceptually problematic since the conventional level set methods cannot conserve the mass in the sense that no mass is lost or gained [2,4] and thus the material volume will not be constant during the evolution. In fact, significant fluctuations of the material volume can be observed in their numerical results [9]. In the work of Osher and Santosa [11], the Lagrange multiplier was obtained based on a similar assumption that the total material volume can be conserved, but the possible drift of the volume during the iteration was noticed and a Newton's method was used to put the iteration back to the feasible set. In the work of Wang and Wang [23], the material volume was also assumed to be conservative to find the Lagrange multiplier, but a higher or lower multiplier was used to push the volume back to the volume constraint during the evolution. All these methods cannot guarantee that the volume constraint function converge and thus the final solutions may become even infeasible.

Hence, a better way to calculate the Lagrange multiplier is that the Lagrange multiplier is chosen to make the volume constraint exactly satisfied at each iteration. In the present study, based on such a methodology, a bi-sectioning algorithm is proposed to find the Lagrange multiplier ℓ to guarantee that the volume constraint be exactly satisfied during the course of evolution.

4.4. Bi-sectioning algorithm

A bi-sectioning algorithm can be used to determine the value of the Lagrange multiplier ℓ to satisfy the volume constraint at each time step based on the fact that the volume constraint functional $G(\Phi)$ in (41) is a monotonously decreasing function of the Lagrange multiplier ℓ. By using the normal velocities defined in (48), the shape derivative of the volume constraint functional $G(\Phi)$ in Eq. (47) can be re-written as

$$\frac{\mathrm{d}G}{\mathrm{d}t} = \int_{\Gamma_{\mathrm{M}}} (\boldsymbol{\varepsilon}^{\mathrm{T}}\mathbf{C}\boldsymbol{\varepsilon} - \ell)\,\mathrm{d}s \tag{49}$$

from which it can be easily obtained that the $G(\Phi)$ decreases with a large value of ℓ and increases with a low value of ℓ. Hence, the bi-sectioning algorithm can be initialized by setting a lower ℓ_1 and an upper ℓ_2 bound for the Lagrange multiplier. In the present numerical study, it is initially chosen that $\ell_1 = 0$, which will cause a maximum volume increase, and $\ell_2 = 10^5$, which may generate a significant volume decrease since all of the normal velocities may become negative due to the relatively small strain energy density and the free boundary thus moves inwardly. The interval which bounds the Lagrange multiplier is halved and the Lagrange multiplier is given by

$$\ell = (\ell_1 + \ell_2)/2 \tag{50}$$

from which the normal velocities v_{n} in (48) as well as the extension velocities, which will be discussed later, can be determined and thus the generalized expansion coefficients $\boldsymbol{\alpha}$ in (37) can be updated. Since the implicit level set function $\Phi(\mathbf{x}, t)$ in (24) and the material volume $V(\Phi)$ in (5) can also be determined, the value of the volume constraint function $G(\Phi)$ in (41) will be finally obtained. Therefore, the interval which bounds the Lagrange multiplier can be repeatedly halved until its size is less than the convergence criteria, similar to the conventional bi-sectioning algorithm used in the popular element-based SIMP method [32]. According to our numerical practice, this bi-sectioning algorithm is effective with a fast convergence speed.

By using this bi-sectioning algorithm, the material volume constraint can be exactly satisfied during the iteration and thus the material volume can be constant during the evolution of the moving free boundary. Hence, the present normal velocities may become a kind of mass conserving velocities and the present level set method can be regarded as mass conservative.

4.5. Shape optimization

According to the present steepest gradient method, for the optimal design, we have

$$v_n = \boldsymbol{\varepsilon}^{\mathrm{T}}\mathbf{C}\boldsymbol{\varepsilon} - \ell = 0 \tag{51}$$

which implies that the strain energy density is a constant everywhere along the optimal free boundary Γ_{M} since the Lagrange multiplier ℓ is time-dependent only. This is also a target pursued by the classical shape optimization methods based on a shape sensitivity analysis [62,67]. Hence, the present level set model can perform not only the free boundary-based topology optimization but also the shape optimization.

In the classical shape optimization, a key concept is the "speed function" V_{n} of the optimality condition associated with a small variation in the boundary shape in the normal direction n. In general, it is necessary that

$$V_n(\mathbf{x}) = 0 \tag{52}$$

everywhere on the design boundary of the optimal structure. Physically, this indicates that the mutual energy form of the elastic structure reaches a constant value on the boundary [62]. In most shape optimization applications, a Lagrangian formulation of boundary propagation was used to achieve the optimality condition and

obtain an optimal shape of the structure [62,67]. The moving boundary is usually discretized with a set of design variables directly controlling the exterior and interior boundaries. Only an explicit boundary representation method is used and the boundary changes can be accomplished only if the connectivity of the boundaries does not change since there is a sever limitation that only a structure of a fixed topology can be optimized. In the present level set-based optimization model, both shape and topology can be optimized simultaneously. The whole design domain is implicitly represented by a level set function $\Phi(\mathbf{x})$ and the moving free boundary is represented by the zero level sets, which may experience significant topological changes such as developing sharp corners, breaking apart, merging together or even disappearing. Furthermore, topological changes in a structure can be easily captured. Hence, the present level set-based optimization method can be more powerful than the classical shape optimization methods.

4.6. Extension velocities

As aforementioned, the normal velocity v_n defined at the free boundary must be extended, either to the whole design domain D [8] or to a narrow band around the free boundary [4], in the level set methods. The choice of an extension velocity method is crucial since it can directly influence the overall efficiency of the level set method [16,23,68].

There are many approaches to constructing the extension velocity $v_n^e(\mathbf{x})$ in the literature. In the original level set method introduced by Osher and Sethian [1], a natural construction of an extension velocity field was obtained, in which a signed distance function was used as a level function. In many fluid simulations, the fluid velocity was chosen as the extension velocity [69,70]. An approach using less physical quantity to build an extension velocity field was developed by Sethian and Strain [71], in which a numerical simulation of dendritic solidification with a jump condition across the interface was presented. When there is no physically meaningful choice available, the extension velocity field was suggested to be constructed by extrapolating the velocity from the front by some researchers [72], which requires the location of the closest grid point. The idea of letting the extension velocity be a constant along the curve normal to the interface is quite natural, however, constructing this extension velocity in the whole domain requires quite considerable effort [2,17]. Hence, a fast extension method was proposed by Adalsteinsson and Sethian [73], which preserves the signed distance in a narrow band around the zero level set curve by assuming the normal velocity be constant along the normal. More recently, in structural topology optimization, the extension velocities were obtained by extending the strain energy density at the free boundary to the whole design domain by Allaire et al. [8]. Since the velocity and the normal may be not smooth at the front, another PDE solving procedure was introduced. It should be noted that in these extension velocity methods a signed distance function was often used as the level set function and therefore the level set function must be reinitialized periodically to preserve the signed distance. Hence, a time-consuming PDE solving procedure [2] may be required and the accuracy and efficiency of the level set methods may be deteriorated [2,46].

In the present study, a physically meaningful extension velocity method without the additional PDE solving procedure is presented for structural shape and topology optimization. According to Eq. (48), a natural extension of the normal velocity v_n at the free boundary can be obtained if the strain field $\boldsymbol{\varepsilon}(\mathbf{u})$ is extended to the entire design domain D by assuming $\boldsymbol{\varepsilon}(\mathbf{u}) = 0, \mathbf{u} \in (D \backslash \Omega)$. Nevertheless, this extension will introduce an apparent discontinuity in the extension velocity at the free boundary since the strain field is not continuous across the free boundary. To guarantee a smooth progress of the free boundary, this discontinuity should be eliminated. Hence, a linear smoothing filter is introduced in the narrowband region around the free boundary, which is defined as

$$\Xi = \{\mathbf{x} \in \mathbb{R}^d || \Phi(\mathbf{x})| \leqslant \Delta\}, \tag{53}$$

where Δ is the bandwidth. The extension velocity v_n^e in the narrowband is smoothed as $\widehat{v_n^e}$ by using a simple linear filter (radially linear 'hat' kernel popular in the SIMP-based topology optimization [32,33]) to achieve an excellent smoothing effect [23,61], which can be written as

$$\widehat{v_n^e}(\mathbf{x}) = k^{-1}(\mathbf{x}) \sum_{\mathbf{p} \in N(\mathbf{x})} w(\|\mathbf{p} - \mathbf{x}\|) v_n^e(\mathbf{x}), \tag{54}$$

where

$$w(\|\mathbf{p}-\mathbf{x}\|) = r_{\min} - \|\mathbf{p}-\mathbf{x}\|, \tag{55}$$

$$k(\mathbf{x}) = \sum_{\mathbf{p}\in N(\mathbf{x})} w(\|\mathbf{p}-\mathbf{x}\|) \tag{56}$$

in which $N(\mathbf{x})$ is the neighborhood of $\mathbf{x} \in \Xi$ in the filter window and $r_{\min}$ the window size. Hence, the overall extension velocity is obtained as

$$v_n^e = v_n^e(\mathbf{x}) = \begin{cases} \boldsymbol{\varepsilon}^T \mathbf{C}\boldsymbol{\varepsilon} - \ell & \forall \mathbf{x} \in \mathbb{R}^d | \Phi(\mathbf{x}) < -\Delta, \\ \widehat{v_n^e}(\mathbf{x}) & \forall \mathbf{x} \in \Xi, \\ -\ell & \forall \mathbf{x} \in \mathbb{R}^d | \Phi(\mathbf{x}) > \Delta. \end{cases} \tag{57}$$

Using this extension velocity field v_n^e, $\mathbf{B}(\boldsymbol{\alpha})$ can be obtained from Eq. (35) at each time step and thus the generalized expansion coefficients $\boldsymbol{\alpha}$ in (37) can be updated. The motion of the free boundary can be obtained by using the updated implicit level set function $\Phi(\mathbf{x}, t)$ in (24). This procedure should be repeated until the convergence criteria have been reached.

Furthermore, the resulting extension velocities are physically meaningful since both the strain energy density and the mass-conserving Lagrange multiplier are closely associated with physics and geometry. As illustrated in the present numerical examples, the evolution of the level set function with this extension velocity field may finally lead to the creation of new holes at the sites inside the material domain where materials are inefficiently used, similar to the evolutionary structural optimization approach [35], the bubble method [74], and the topological gradient method [26]. This can be a significant improvement over the conventional level set methods, which only allow limited topological changes by splitting or merging connected components [37].

5. Numerical examples and discussion

In this section, numerical examples in two dimensions are presented to illustrate the performance and success of the present extended level set method for structural shape and topology optimization. Unless stated otherwise, all the units are consistent and the following parameters are assumed as: the Young's elasticity modulus $E = 1$ for solid materials, $E = 1 \times 10^{-5}$ for void materials, and Poisson's ratio $v = 0.3$. The implicit level set function $\Phi(\mathbf{x})$ is initially chosen as a signed distanced function by using the present RBF modeling from a set of given points and no extra efforts such as reinitialization are made to keep this property during the optimization process.

For all examples, a fixed rectilinear mesh is specified over the entire design domain for finite element (FE) analysis of the structures. The FE analysis is based on the bilinear rectangular elements and an "ersatz material" approach, which is well-known in topology optimization that can be rigorously justified in some cases [8,75]. In numerical practice of the "ersatz material" approach, material density is assumed to be piecewise constant in each element and is adequately interpolated in those elements cut by the zero level set function (the free boundary). It is also assumed that the knots of the RBFs are coincidental to the nodes of the rectilinear mesh. Furthermore, $\Delta = 1$ grid size for the bandwidth size, $r_{\min} = 1.2$ grid size for the filter window size, and $c = 10^{-4}$ for the free shape parameter in the MQ RBFs (10). It should be noted that the choice of the free shape parameter may affect the accuracy of the final optimization results and a more detailed study can be found in the work of the authors [16]. The present algorithm is terminated when the relative difference between two successive objective function values is less than 10^{-5} or when the given maximum number of iterations has been reached. The topologies are given in black-and-white form based on the scalar value of the implicit function $\Phi(\mathbf{x})$, as defined in Eq. (1). All the CPU time is based on a desktop computer under the MATLAB environment with an Intel Pentium IV processor of 3.00 GHz clock speed.

5.1. Short cantilever beam

The minimum compliance design problem of a short cantilever beam is shown in Fig. 1. The whole design domain D is a rectangle of size 2×1 with a fixed boundary ∂D (zero displacement boundary condition) on the

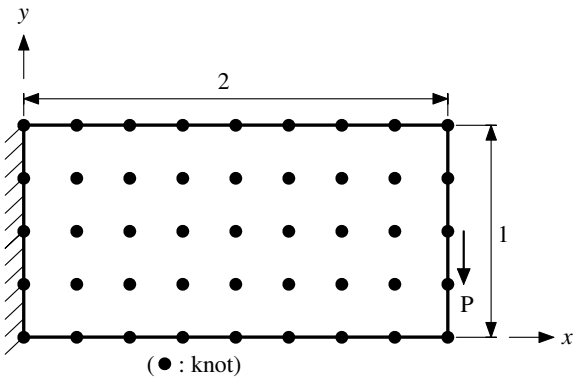

Fig. 1. Definition of the minimum compliance design problem of a short cantilever beam.

left side and a unit vertical point load $P = 1$ applied at a fixed non-homogeneous Neumann boundary ∂D_N, the middle point of the right side. The specified material volume fraction is $\zeta = 0.5$. The distribution of the RBF knots is illustrative only. It should correspond to the nodes distribution of the underlying FE mesh for structural analysis.

Fig. 2 displays the evolution of an optimal topology of the short cantilever beam with an initial design as shown in Fig. 2(a) by using the present level set method with a 80×40 FE mesh and a time step size $\tau = 10^{-4}$. It can be seen that significant topological changes have been achieved and the final design as shown in Fig. 2(f) is similar to those reported in the literature [8,23,25] using the conventional level set methods. Hence, optimal topologies can also be obtained by using the present extended level set method, rather than by using the upwind schemes in the conventional level set methods [2,4]. The evolution of the corresponding moving free boundary Γ_M is shown in Fig. 3, in which the free boundary is approximately depicted by piecewise lines and

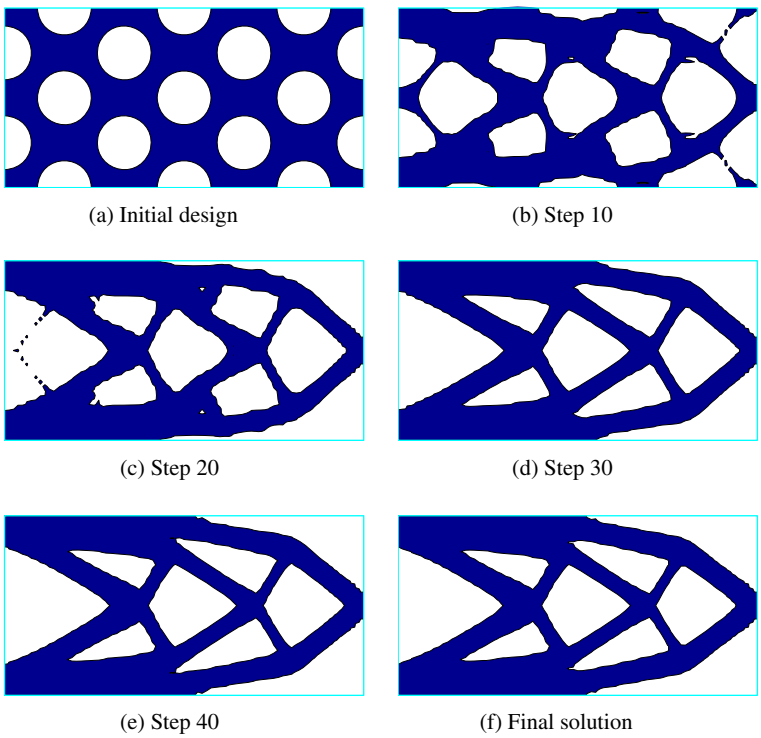

(a) Initial design (b) Step 10

(c) Step 20 (d) Step 30

(e) Step 40 (f) Final solution

Fig. 2. Evolution of an optimal solution for the short cantilever beam.

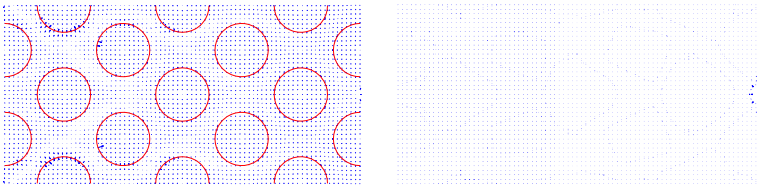

(a) Initial design

(f) Final solution

Fig. 3. Evolution of the moving free boundary of the short cantilever beam.

the extension ve…each knot are indicated by the arrows. According to the present mass-conserving extension velo…ving free boundary can develop sharp corners, break apart, merge together and disappear in…y during the course of evolution. Although the maximum velocity is located on the free…itial design, the location is rapidly shifted to the location inside the material domain a…s due to the present steepest gradient optimization method and a stress concentrati…on. In the optimal solution, as shown in Fig. 4, the scalar normal velocities at the…zero, which agrees well with the theoretical prediction that the normal veloc…ary [8] and indicates that a shape optimization is also achieved.

…of the objective function and the volume function for the short cantile…liance of the optimal solution is significantly better than that of the …in a fast and stable way due to the present level set-based optimi…me constraint ($V/V_0 = 0.5$) can almost be exactly satisfied during …sign possesses a higher material volume ($V/V_0 = 0.578$) and is …t study this is achieved by choosing an appropriate Lagrange …than based on the problematic assumption that the material …n [9,11,16]. Hence, the optimal solutions can be guaranteed

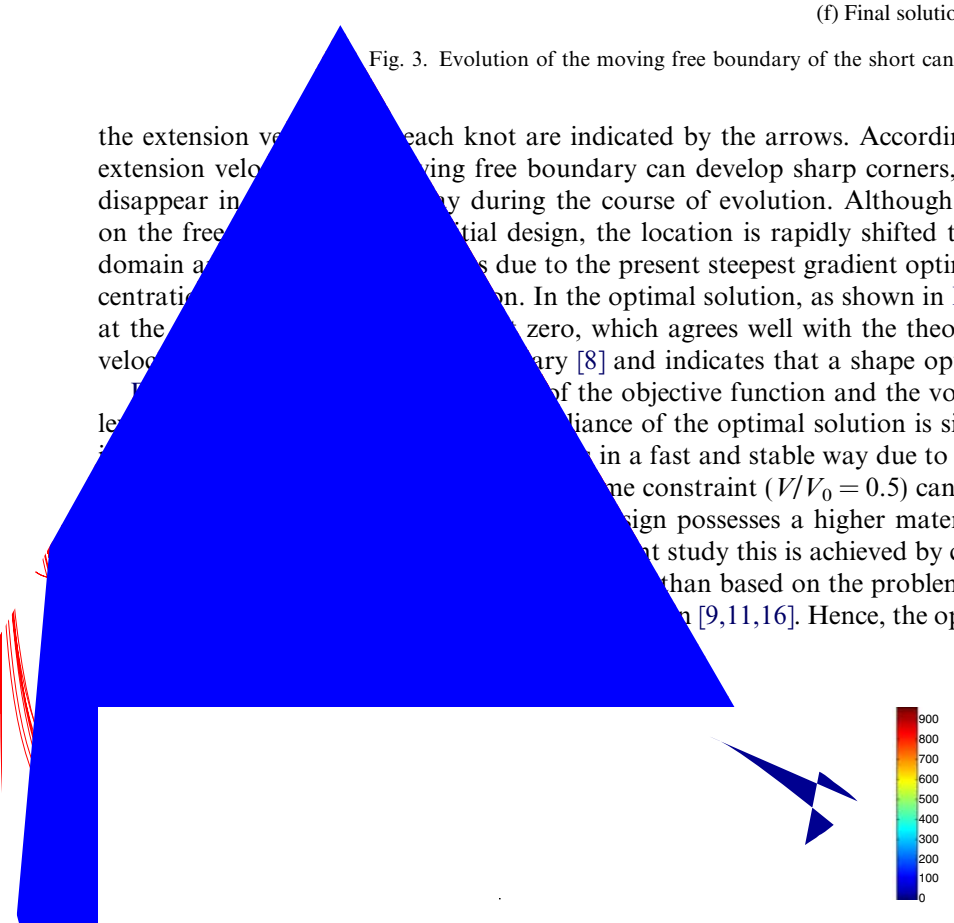

Fig. 4. Scalar extension velocity field ($v_n \geqslant 0$) for an optimal solution of the short cantilever beam.

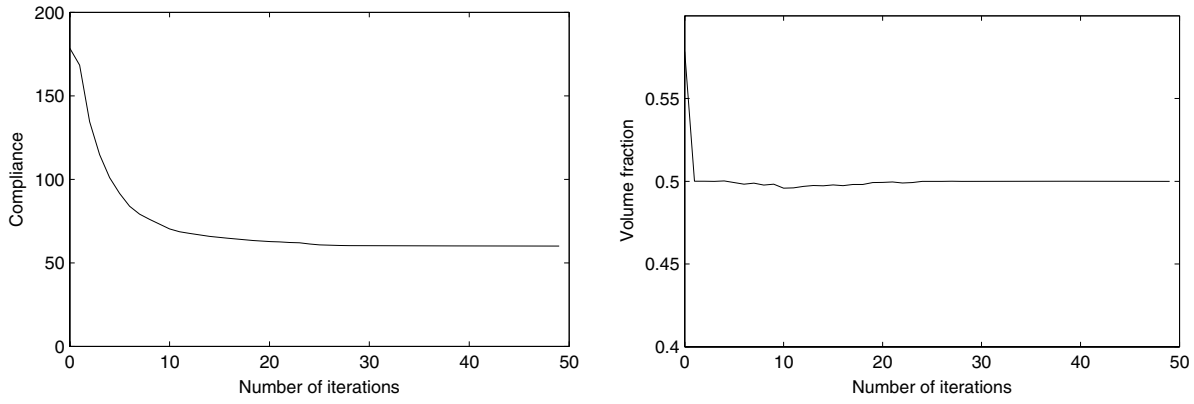

(a) Objective function (b) Volume

Fig. 5. Convergence of the objective function and the volume for the short cantilever beam.

to be feasible and the underlying level set method may become mass conservative to make the material volume constant during the iterations. Furthermore, the conventional level set methods for shape and topology optimization [8,9,11–13,16,23] may also become mass conservative by applying the present mass-conserving velocities.

For the purpose of comparison, this shape and topology optimization problem is solved again by using a conventional level set model in [20] and the present mass-conserving extension velocities. In the level set model, a second-order ENO (essentially non-oscillatory) upwind scheme is used for the propagation of the free boundary and a third-order reinitialization algorithm is adopted to minimize the numerical diffusion around the location of the original interface [6], and an aggressive CFL number of 1 is used to drive a fast convergence. Reinitialization as an auxiliary step is performed every 5 times of transport and the maximum number of iterations is specified as 200. The final solutions are shown in Fig. 6. It can be seen that the final topology is similar to the optimal topology shown in Fig. 2(f), however, shape optimization is not completed since there is an apparent discrepancy between the free boundary shown in Fig. 6(a) and the zero scalar velocity curve shown in Fig. 6(b). It is thus suggested that the convergence of both the shape and the topology has not been reached. The convergence speed of the objective function and the material volume is shown in Fig. 7. As expected, the material volume shown in Fig. 7(b) is almost exactly constant during the iterations, different from the conventional level set methods in the literature [8,9,11–13,16,23]. Furthermore, the objective function decreases in a quite stable way, which justifies the use of an aggressive CFL number in this case, but it converges significantly slower than using the present extended level set method. This is a typical drawback of a CFL-dependent conventional level set model, as aforementioned. Hence, the present method may significantly excel the conventional level set methods in computational efficiency for shape and topology optimization.

Nucleation of some new holes can be observed in Figs. 2(b) and (c), which suggests that the present level set method has the capability of nucleation of new holes. To further demonstrate this capability, shape and

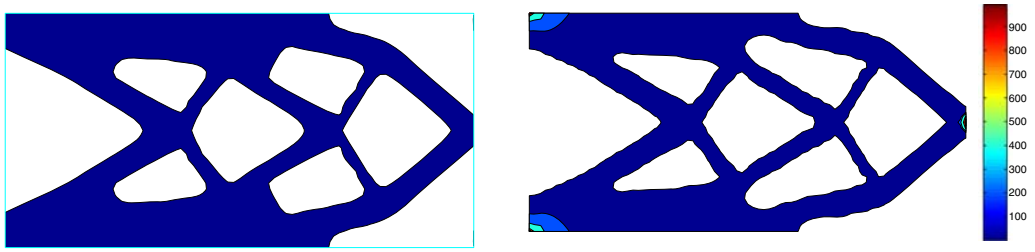

(a) Final topology (b) Scalar extension velocity field ($v_n \geqslant 0$)

Fig. 6. Final solutions for the short cantilever beam using a conventional level set method.

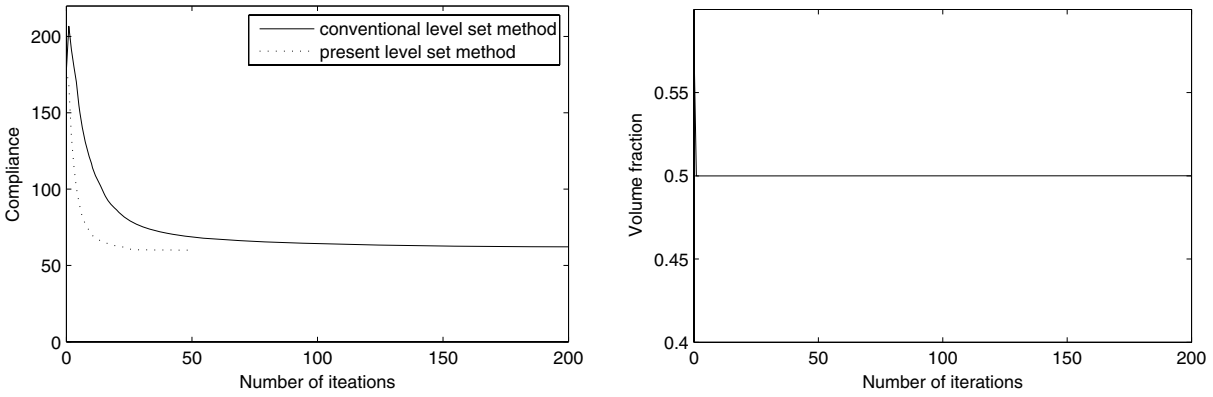

(a) Objective function (b) Volume

Fig. 7. Convergence of the objective function and the volume for the short cantilever beam using a conventional level set method.

topology optimization is performed again starting from a design without a hole. The initial design and the final solution are shown in Fig. 8. It can be seen that although the initial design is without a hole, the final solution can also be similar to the optimal solution with holes shown in Fig. 2(f) using an initial design with holes. Hence, the initial design does not influence the final solution too significantly since the maximum principle [4] is not obeyed rigorously and topological changes to create new holes are allowed for in the present extended level set method. As a result, the present method is less sensitive to initialization than the conventional level set methods [8,25]. Fig. 9 shows the convergence speed of the objective function and the material volume function. Since the objective function decreases significantly with the time advancement in a stable

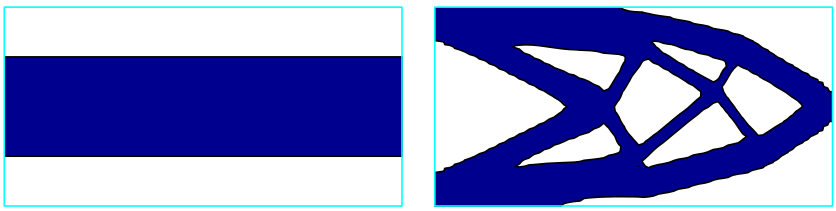

(a) Initial design (b) Final solution

Fig. 8. Final solution for the short cantilever beam using an initial design without a hole.

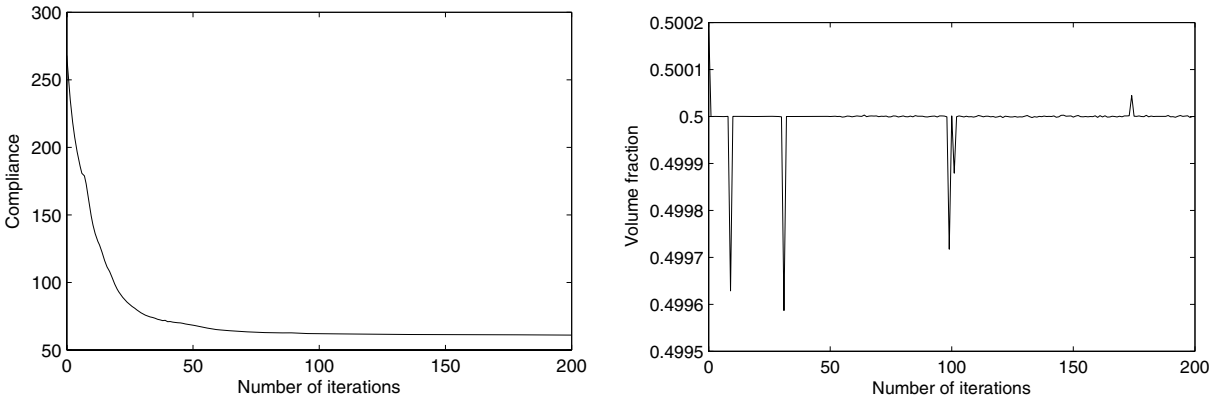

(a) Objective function (b) Volume

Fig. 9. Convergence of the objective function and the volume for the short cantilever beam using an initial design without a hole.

manner, the nucleation of new holes can be justified. Again, from Fig. 9(b) it can be seen that the material volume constraint can be almost exactly satisfied during the iterations. Furthermore, shape and topology optimization using an initial design with a material domain occupying the upper half of the design domain is also performed and similar observations can be made, according to the final solution shown in Fig. 10 and the convergence speed shown in Fig. 11. In the conventional level set methods, the nucleation of new holes is not allowed for and thus a bubble or topological gradient method has to be incorporated into the level set methods, as shown in [25,26,74]. Since both the topological and shape derivatives are used in a modified level set method, it would be quite difficult to switch between them in an automatic way [25,26]. Moreover, it can be quite complicated for the topological derivative to handle surface functions [37]. In the present extended level set method, the topological derivative is not used and the creation of new holes can be fulfilled by using the shape derivative only.

Although the present extended level set method can satisfy the volume constraint at each iteration, it may experience difficulties to handle an initial design quite far away from the feasible domain with a fixed volume constraint. For example, if an initial design is with a much higher material volume fraction than the pre-specified volume constraint, to satisfy the volume constraint after a single step, too significant topological changes may have to be experienced and quite unstable solutions may thus be produced. To deal with this situation, a minor modification to the present mass-conserving Lagrange multiplier is developed by combining the present method with the method in [16,23] using a fixed Lagrange multiplier to decrease the material volume. A neighborhood of the feasible domain is pre-specified (for this example, a volume fraction range of $[0.4, 0.6]$ for the required volume fraction 0.5 is used as the neighborhood). When the material volume falls inside this range, the variable Lagrange multiplier is determined by the present bi-sectioning algorithm as aforementioned. However, when the material volume falls outside this range, a fixed Lagrange multiplier ($\ell = 20$ for this example) with a relatively large or small positive volume is used to drive the material volume towards the neighborhood of the feasible domain [16,23]. This idea is here illustrated by using an initial design with a heavy

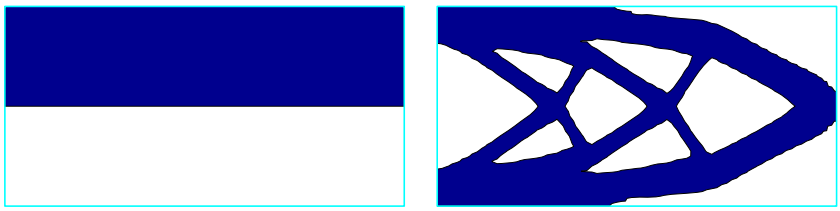

(a) Initial design (b) Final solution

Fig. 10. Final solution for the short cantilever beam using another initial design without a hole.

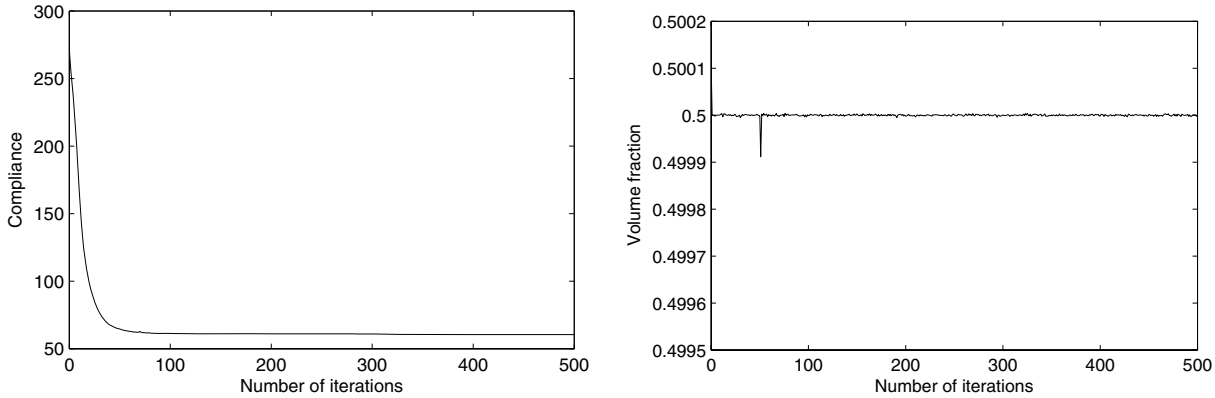

(a) Objective function (b) Volume

Fig. 11. Convergence of the objective function and the volume for the short cantilever beam using another initial design without a hole.

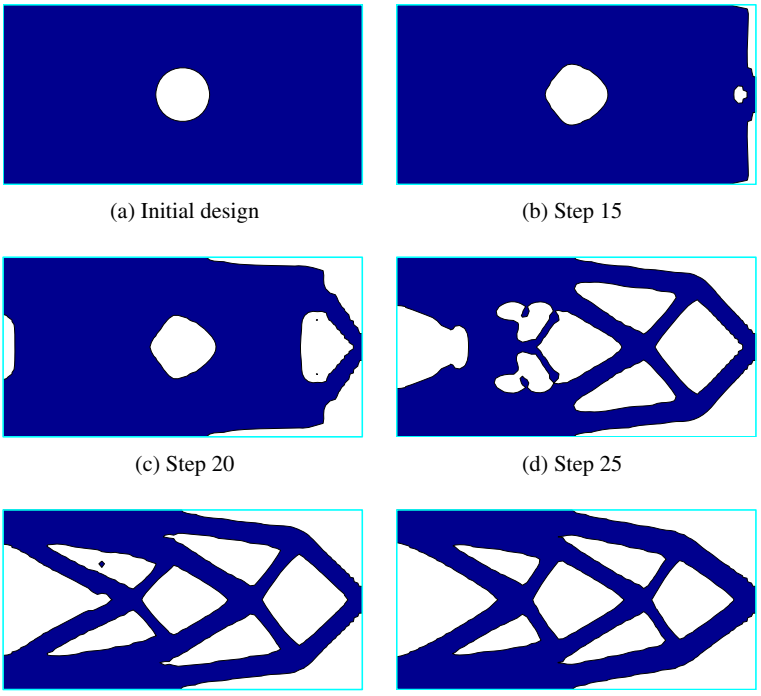

(a) Initial design (b) Step 15

(c) Step 20 (d) Step 25

(e) Step 30 (f) Final solution

Fig. 12. Evolution of an optimal topology using an initial design with a central hole.

material volume fraction of 0.9649 as shown in Fig. 12(a). The initial design, the intermediate results and the final solution are shown in Fig. 12. It can be seen that smooth topological changes have been reached and a final solution similar to the previous one can be achieved. Furthermore, it can be seen from Fig. 13 that convergence of both the objective function and the volume constraint function from the initial infeasible domain to the feasible domain (starting from step 25) are stable, though the initial design possesses a much lower compliance value than the optimal solution due to its much higher material volume. Therefore, the infeasible initial design quite far away from the feasible domain is driven towards the feasible domain successfully and the present method with this modification can be initial design-independent.

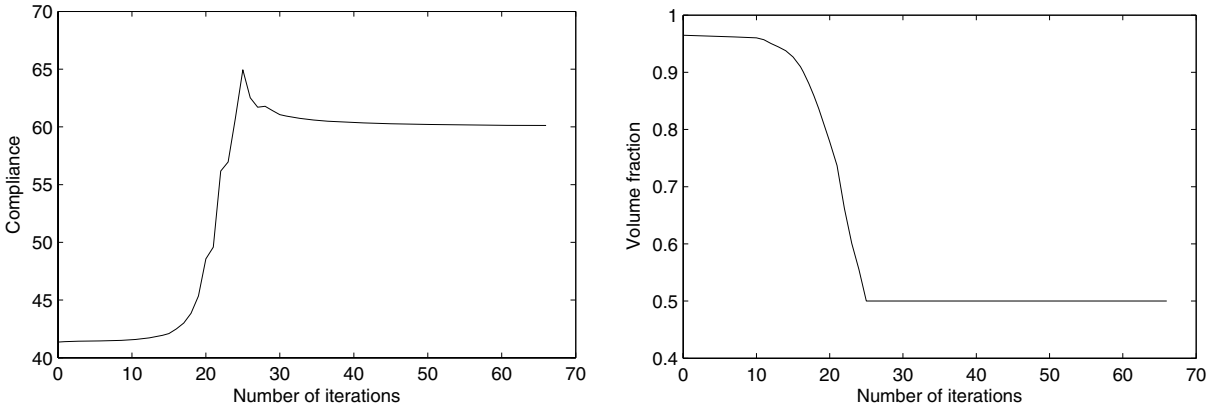

(a) Objective function (b) Volume

Fig. 13. Convergence of the objective function and the volume for the short cantilever beam using an initial design with a central hole.

The initial designs do not affect the final design significantly in the present extended level set method, however, the computational efficiency may be greatly affected. Table 1 displays the effect of the initial designs on the computation time. It can be seen that the present method converges fastest with an initial design with holes and converges slowest with an initial design without a hole and quite different from the final design, since topological changes can be more easily handled by decreasing the number of holes rather than by creating new holes. This is consistent with the observations made in [25,26] and may justify the use of heavily perforated initial designs in [7,12,19].

5.2. Michell type structure

The present extended level set method is finally applied to the classical Michell type structure problem, in which a theoretical Michell's solution is available in the literature [34–36,76], as shown in Fig. 14(b). The whole design domain D is a rectangle of size $L \times H$, the two bottom corners have the pinned supports, and a unit vertical point force P is applied at the middle point of the bottom side. As shown in Fig. 14(b), the theoretical optimum topology consists of two 45° arms extending from the supports towards an approximately 90° central fan section which extends upwards from the point of application of the force. In the present study, it is assumed that $L = 2$, $H = 1.2$, $P = 1$, and a pre-specified material volume fraction $\zeta = 0.3$. The domain D is discretized with a fixed rectangular mesh of 80×48 and a timestep size of $\tau = 10^{-3}$ is adopted.

A heavily perforated structure with a material volume fraction of 0.7023 as shown in Fig. 15(a) is chosen to achieve a rapid convergence speed. The present extended level set method without further modifying the Lagrange multiplier as just suggested is applied. The corresponding evolution history of the final shape and topology is shown in Fig. 15. It can be seen that the final solution can be reached rapidly. Hence, the present method without further modifying the Lagrange multiplier can be applicable to infeasible designs with multiple holes, though the initial material volume fraction of 0.7023 is significantly larger than the required volume fraction of 0.3 for this problem. For this case, using a problem-dependent fixed Lagrange multiplier, which may cause mathematical complexity in determining its appropriate value, to drive the material volume towards the feasible domain is not needed. Furthermore, the final topology consisting of two arms and a central fan section is quite similar to the theoretical optimum topology shown in Fig. 14(b) and therefore the effectiveness and accuracy of the present method is again illustrated. The convergence of the objective function and the volume constraint function is shown in Fig. 16. Although the objective function may

Table 1
Effect of initial designs for the short cantilever beam

Initial design	$J_{\min}$	N_{it}	T_0 (s)
Fig. 2(a)	60.0696	50	2.1964e + 003
Fig. 8(a)	60.9703	200	7.0858e + 003
Fig. 10(a)	60.4885	500	1.7589e + 004
Fig. 12(a)	60.1189	67	2.3940e + 003

$J_{\min}$: minimum compliance; N_{it}: total number of iterations; T_0: total CPU time.

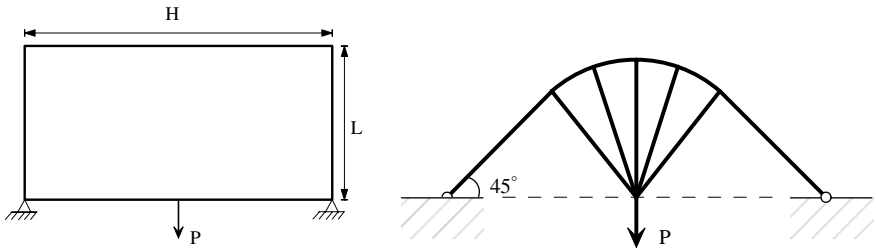

(a) Design domain (b) A Michell type structure

Fig. 14. Optimal design problem for Michell type structures with fixed supports.

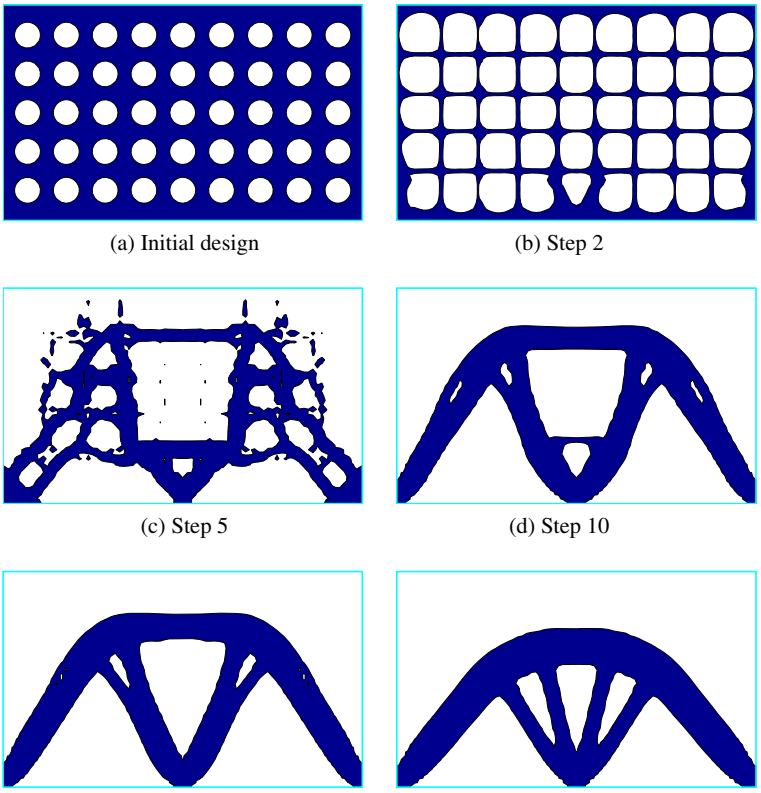

(a) Initial design (b) Step 2

(c) Step 5 (d) Step 10

(e) Step 20 (f) Final solution

Fig. 15. Evolution of an optimal solution for the Michell type structure.

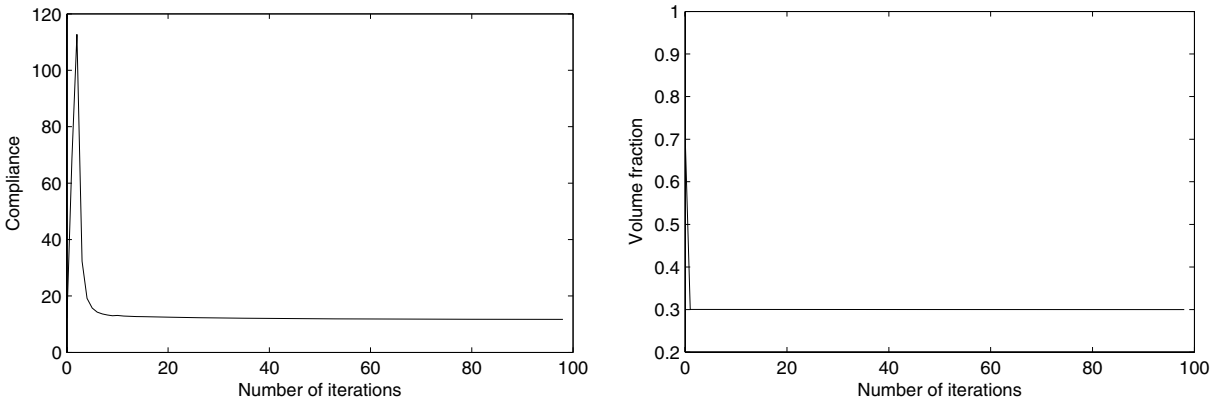

(a) Objective function (b) Volume

Fig. 16. Convergence of the objective function and the volume for Michell type structure.

increase in the early iterations due to the large number of bars to be broken to satisfy the volume constraint, it finally converges in a smooth and stable way. Again, as expected, Fig. 16(b) displays that the volume constraint can be almost exactly satisfied during the course of evolution. It should also be noted that the present method can be more powerful since it can also perform the classical shape optimization, as shown in Fig. 17, in which the zero scalar velocity curve corresponds to the free boundary of the final solution shown in Fig. 15(f) almost exactly.

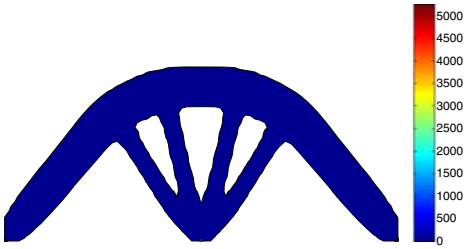

Fig. 17. Scalar extension velocity field ($v_n \geqslant$

6. Conclusions

An extended level set method for classical shape and topology optimization is proposed based on the popular radial basis functions. The implicit level set function is approximated by using the RBF implicit modeling with multiquadric splines. Because of the global smoothness of this representation, a high level of accuracy and smoothness of the implicit function is achieved. Furthermore, the Hamilton–Jacobi PDE is discretized into a mathematically more convenient coupled ODE system and the original time dependent initial value problem becomes a relatively simple time-dependent interpolation problem. It turns out that a relatively smooth level set evolution can be maintained without reinitialization due to the use of global support RBFs. A practical implementation of the present method is developed for solving a class of energy-based optimization problems, in which inaccurate solution to the original Hamilton–Jacobi PDE may be justified and nucleation of new holes inside the material domain is allowed for. As a result, the constraints on the temporal and spatial discretizations can be significantly relaxed by satisfying the optimization requirements only and the direct consequence of time stability problem can be circumvented due to the globally smooth RBF implicit modeling. Hence, a rapid convergence to the final design insensitive to initial guesses becomes possible.

The present extended level set method is applied to the classical shape and topology optimization. The proposed shape and topology optimization process operates on the implicit level set function represented by the RBF implicit modeling and uses a steepest gradient method and shape derivatives to find the decent direction of the normal velocity for the minimization of an objective function. By using the present bi-sectioning algorithm, the Lagrange multiplier can be accurately obtained and the present extended level set method can thus be mass conservative. It is also highlighted that the classical shape optimization can be performed simultaneously. By using the global strain energy density field and a linear smoothing filter, the normal velocity at the free boundary is naturally and smoothly extended to the whole design domain without using an additional PDE solving procedure. This proposed method is implemented in the framework of shape and topological optimum of minimum compliance design and its higher efficiency over the conventional level set methods is illustrated. Numerical examples of 2D structures are chosen to show the success of the present method in accuracy, convergence speed and insensitivity to initial designs. Compared with the conventional level set methods, the present method can either generate similar optimal designs rapidly without reinitialization or largely eliminate the dependency on initial designs due to its capability in nucleation of new holes inside the material domain. It is suggested that the introduction of the radial basis functions into the conventional level set methods possesses promising potentials.

Acknowledgments

This research work is partly supported by the Research Grants Council of Hong Kong SAR (Project No. CUHK4164/03E), a Post-doctoral Fellowship from the Chinese University of Hong Kong (No. 04/ENG/1), the Natural Science Foundation of China (NSFC) (Grant Nos. 50128503 and 50390063), a Research Fellowship from the National University of Singapore, which the authors gratefully acknowledge. The insightful comments of the reviewers' as well as Professor Osher's are cordially appreciated.

References

[1] S. Osher, J.A. Sethian, Front propagating with curvature dependent speed: algorithms based on Hamilton–Jacobi formulations, Journal of Computational Physics 78 (1988) 12–49.
[2] J.A. Sethian, Level Set Methods and Fast Marching Methods, second ed., Cambridge Monographs on Applied and Computational Mathematics, Cambridge University Press, Cambridge, UK, 1999.
[3] S. Osher, R.P. Fedkiw, Level set methods: an overview and some recent results, Journal of Computational Physics 169 (2001) 463–502.
[4] S.J. Osher, R.P. Fedkiw, Level Set Methods and Dynamic Implicit Surfaces, Springer, New York, 2002.
[5] S. Osher, N. Paragios, Geometric Level Set Methods in Imaging, Vision, and Graphics, Springer, New York, 2003.
[6] R. Tsai, S. Osher, Level set methods and their applications in image science, Communications in Mathematical Sciences 1 (4) (2003) 623–656.
[7] J.A. Sethian, A. Wiegmann, Structural boundary design via level set and immersed interface methods, Journal of Computational Physics 163 (2) (2000) 489–528.
[8] G. Allaire, F. Jouve, A.-M. Toader, Structural optimization using sensitivity analysis and a level-set method, Journal of Computational Physics 194 (2004) 363–393.
[9] M.Y. Wang, X. Wang, D. Guo, A level set method for structural topology optimization, Computer Methods in Applied Mechanics and Engineering 192 (2003) 227–246.
[10] M.Y. Wang, X. Wang, PDE-driven level sets, shape sensitivity and curvature flow for structural topology optimization, Computer Modeling in Engineering & Sciences 6 (4) (2004) 373–395.
[11] S. Osher, F. Santosa, Level-set methods for optimization problems involving geometry and constraints: frequencies of a two-density inhomogeneous drum, Journal of Computational Physics 171 (2001) 272–288.
[12] M.Y. Wang, X.M. Wang, Color level sets: a multi-phase method for structural topology optimization with multiple materials, Computer Methods in Applied Mechanics and Engineering 193 (6–8) (2004) 469–496.
[13] M.Y. Wang, X. Wang, A level-set based variational method for design and optimization of heterogeneous objects, Computer-Aided Design 37 (2005) 321–337.
[14] L.A. Vese, T.F. Chan, A multiphase level set framework for image segmentation using the Mumford and Shah model, International Journal of Computer Vision 50 (2002) 271–293.
[15] Q. Xia, M.Y. Wang, S.Y. Wang, S.K. Chen, Semi-lagrangian method for level-set based structural topology and shape optimization, Structural and Multidisciplinary Optimization (in press).
[16] S.Y. Wang, M.Y. Wang, Radial basis functions and level set method for structural topology optimization, International Journal for Numerical Methods in Engineering 65 (12) (2006) 2060–2090.
[17] D. Peng, B. Merriman, S. Osher, H. Zhao, M. Kang, A PDE-based fast local level set method, Journal of Computational Physics 155 (1999) 410–438.
[18] P. Gómez, J. Hernández, J. López, On the reinitialization procedure in a narrow-band locally refined level set method for interfacial flows, International Journal for Numerical Methods in Engineering 63 (10) (2005) 1478–1512.
[19] G. Allaire, F. Jouve, A.-M. Toader, Structural optimization using sensitivity analysis and a level-set method, Journal of Computational Physics 194 (2004) 363–393.
[20] I.M. Mitchell, A toolbox of level set methods, Technical Report TR-2004-09, Department of Computer Science, University of British Columbia, Canada, 2004.
[21] S. Osher, C.-W. Shu, High-order essentially nonoscillatory schemes for Hamilton–Jacobi equations, SIAM Journal on Numerical Analysis 28 (1991) 907–922.
[22] G.-S. Jiang, D. Peng, Weighted ENO schemes for Hamilton–Jacobi equations, SIAM Journal on Scientific Computing 21 (2000) 2126–2143.
[23] S.Y. Wang, M.Y. Wang, A moving superimposed finite element method for structural topology optimization, International Journal for Numerical Methods in Engineering 65 (11) (2006) 1892–1922.
[24] E. Haber, A. multilevel, level-set method for optimizing eigenvalues in shape design problems, Journal of Computational Physics 198 (2004) 518–534.
[25] G. Allaire, F.D. Gournay, F. Jouve, A.-M. Toader, Structural optimization using topological and shape sensitivity via a level set method, Internal Report 555, Ecole Polytechnique, France, 2004.
[26] M. Burger, B. Hackl, W. Ring, Incorporating topological derivatives into level set methods, Journal of Computational Physics 194 (2004) 344–362.
[27] X. Wang, Y. Mei, M.Y. Wang, Incorporating topology/phase derivatives into level set methods for optimization of solids, in: WISDOM 2004-Warsaw International Seminar on Design and Optimal Modeling, Warsaw, Poland, 2004.
[28] M.Y. Wang, P. Wei, Topology optimization with level set method incorporating topological derivative, in: 6th World Congress on Structural and Multidisciplinary Optimization, Rio de Janeiro, Brazil, 2005.
[29] M.D. Buhmann, Radial Basis Functions: Theory and ImplementationsCambridge Monographs on Applied and Computational Mathematics, vol. 12, Cambridge University Press, New York, NY, 2004.
[30] A.-D. Cheng, M.A. Golberg, E.J. Kansa, G. Zammito, Exponential convergence and H-c multiquadric collocation method for partial differential equations, Numerical Methods for Partial Equations 19 (5) (2003) 571–594.
[31] E.J. Kansa, H. Powerb, G.E. Fasshauerc, L. Ling, A volumetric integral radial basis function method for time-dependent partial differential equations I. Formulation, Engineering Analysis with Boundary Elements 28 (2004) 1191–1206.

[32] O. Sigmund, A 99 line topology optimization code written in MATLAB, Structural and Multidisciplinary Optimization 21 (2) (2001) 120–127.
[33] M.P. Bendsøe, O. Sigmund, Topology Optimization: Theory, Methods and Applications, Springer, Berlin, 2003.
[34] A.G.M. Michell, The limits of economy of material in frame-structures, Philosophical Magazine 8 (6) (1904) 589–597.
[35] Y.M. Xie, G.P. Steven, A simple evolutionary procedure for structural optimization, Computers & Structures 49 (5) (1993) 885–896.
[36] S.Y. Wang, K. Tai, Bar-system representation method for structural topology optimization using the genetic algorithms, Engineering Computations 22 (2) (2005) 206–231.
[37] M. Burger, Lecture notes on infinite-dimensional optimization and optimal design, Report 285J, University of California, Los Angeles, CA, USA, 2004.
[38] J.C. Carr, R.K. Beatson, J.B. Cherrie, T.J. Mitchell, W.R. Fright, B.C. McCallum, T.R. Evans, Reconstruction and representation of 3D objects with radial basis functions, in: ACM SIGGRAPH 2001, Los Angeles, CA, 2001, pp. 67–76.
[39] B.S. Morse, T.S. Yoo, D.T. Chen, P. Rheingans, K.R. Subramanian, Interpolating implicit surfaces from scattered surface data using compactly supported radial basis functionsSMI'01: Proceedings of the International Conference on Shape Modeling & Applications, IEEE Computer Society, Washington, DC, USA, 2001, pp. 89–98.
[40] R.L. Hardy, Theory and applications of the multiquadric-biharmonic method: 20 years of discovery, Computers & Mathematics with Applications 19 (8/9) (1990) 163–208.
[41] C.A. Micchelli, Interpolation of scattered data: distance matrices and conditionally positive definite, Constructive Approximation 2 (1986) 11–22.
[42] M. Benzi, G.H. Golub, J. Liesen, Numerical solution of saddle point problems, Acta Numerica 14 (2005) 1–137.
[43] R.B. Platte, T.A. Driscoll, Eigenvalue stability of radial basis function discretizations for time-dependent problems, Technical Report 2005-01, Department of Mathematical Sciences, University of Delaware, USA, 2005.
[44] N.K. Madsen, The method of lines for the numerical solution of partial differential equations, ACM SIGNUM Newsletter 10 (4) (1975) 5–7.
[45] K. van den Doel, U. Ascher, On level set regularization for highly ill-posed distributed parameter estimation problems, Journal of Computational Physics 216 (2) (2006) 707–723.
[46] J.C. Ye, Y. Bresler, P. Moulin, A self-referencing level-set method for image reconstruction from sparse Fourier samples, International Journal of Computer Vision 50 (3) (2002) 253–270.
[47] A. Leito, O. Scherzer, On the relation between constraint regularization, level sets, and shape optimization, Inverse Problems 19 (1) (2003) 1–11.
[48] C. Li, C. Xu, C. Gu, M.D. Fox, Level set evolution without re-initialization: a new variational formulation, in: IEEE International Conference on Computer Vision and Pattern Recognition (CVPR), San Diego, 2005, pp. 430–436.
[49] M.D. Greenberg, Advanced Engineering Mathematics, second ed., Prentice-Hall International Inc., Upper Saddle River, NJ, USA, 1998.
[50] H.K. Zhao, T.F. Chan, B. Merriman, S. Osher, A variational level set approach to multiphase motion, Journal of Computational Physics 127 (1996) 179–195.
[51] H.K. Zhao, S. Osher, R. Fedkiw, Fast surface reconstruction using the level set method, in: Proceedings of IEEE Workshop on Variational and Level Set Methods in Computer Vision (VLSM 2001), 2001.
[52] J.E. Solem, N.C. Overgaard, A gradient descent procedure for variational dynamic surface problems with constraints, in: IEEE Proc. Workshop on Variational, Geometric and Level Set Methods in Computer Vision, 2005, pp. 332–343.
[53] P.Y. Papalambros, D.J. Wilde, Principles of Optimal Design: Modeling and Computation, 2nd ed., Cambridge University Press, New York, NY, 2000.
[54] A. Neumaier, Complete search in continuous global optimization and constraint satisfaction, in: A. Iserles (Ed.), Acta Numerica 2004, vol. 13, Cambridge University Press, Cambridge, 2004, pp. 271–369.
[55] S.Y. Wang, K. Tai, M.Y. Wang, An enhanced genetic algorithm for structural topology optimization, International Journal for Numerical Methods in Engineering 65 (1) (2006) 18–44.
[56] T.F. Chan, L.A. Vese, Active contours without edges, IEEE Transactions on Image Processing 10 (2) (2001) 266–277.
[57] M.P. Bendsøe, N. Kikuchi, Generating optimal topologies in structural design using a homogenization method, Computer Methods in Applied Mechanics and Engineering 71 (1988) 197–224.
[58] G.I.N. Rozvany, M. Zhou, T. Birker, Generalized shape optimization without homogenization, Structural Optimization 4 (1992) 250–254.
[59] M.P. Bendsøe, Optimal shape design as a material distribution problem, Structural Optimization 1 (1989) 193–202.
[60] G.I.N. Rozvany, Aims, scope, methods, history and unified terminology of computer-aided topology optimization in structural mechanics, Structural and Multidisciplinary Optimization 21 (2) (2001) 90–108.
[61] M.Y. Wang, S.Y. Wang, Bilateral filtering for structural topology optimization, International Journal for Numerical Methods in Engineering 63 (13) (2005) 1911–1938.
[62] J. Sokolowski, J. Zolesio, Introduction to shape optimization: shape sensitivity analysisSpringer Series in Computational Mathematics, vol. 10, Springer, Berlin, Germany, 1992.
[63] J. Norato, R. Haber, D. Tortorelli, M.P. Bendsøe, A geometry projection method for shape optimization, International Journal for Numerical Methods in Engineering 60 (14) (2004) 2289–2312.
[64] T. Belytschko, T. Black, Elastic crack growth in finite elements with minimal remeshing, International Journal for Numerical Methods in Engineering 45 (5) (1999) 601–620.

[65] T. Strouboulis, K. Copps, I. Babuska, The generalized finite element method, Computer Methods in Applied Mechanics and Engineering 190 (2001) 4081–4193.
[66] T. Belytschko, S.P. Xiao, C. Parimi, Topology optimization with implicit functions and regularization, International Journal for Numerical Methods in Engineering 57 (8) (2003) 1177–1196.
[67] G. Rozvany, Structural Design via Optimality Criteria, Kluwer Academic Publishers, Dordrecht, 1998.
[68] D.F. Richards, M.O. Bloomfield, S. Sen, T.S. Calea, Extension velocities for level set based surface profile evolution, Journal of Vacuum Science and Technology A 19 (4) (2001) 1630–1635.
[69] M. Sussman, P. Smereka, S. Osher, A level-set approach for computing solutions to incompressible two-phase flow, Journal of Computational Physics 114 (1994) 146–159.
[70] C.W. Rhee, L. Talbot, J.A. Sethian, Dynamical behavior of a premixed open V-flame, Journal of Fluid Mechanics 300 (1995) 87–115.
[71] J.A. Sethian, J.D. Strain, Crystal growth and dendritic solidification, Journal of Computational Physics 98 (1992) 231–253.
[72] R. Mallad, J.A. Sethian, B.C. Vemuri, A fast level set based algorithm for topology-independent shape modeling, Journal Mathematical Imaging and Vision 6 (2/3) (1996) 269–290.
[73] D. Adalsteinsson, J.A. Sethian, The fast construction of extension velocities in level set methods, Journal of Computational Physics 148 (1) (1999) 2–22.
[74] H.A. Eschenauer, V.V. Kobelev, A. Schumacher, Bubble method for topology and shape optimization of structures, Structural Optimization 8 (1) (1994) 42–51.
[75] G. Allaire, Shape Optimization by the Homogenization Method, Springer, New York, 2001.
[76] W.S. Hemp, Michell's structural continua, in: Optimum Structures, Clarendon Press, Oxford, 1973 (Chapter 4).